

# Economical Quasi-Newton Self Consistent Field Solver

Samuel A. Slattery, Kshitijkumar Surjuse, and Edward F. Valeev\*

*Department of Chemistry, Virginia Tech, Blacksburg, VA 24061*

E-mail: [efv@vt.edu](mailto:efv@vt.edu)

July 4, 2023

## Abstract

We present an efficient quasi-Newton orbital solver optimized to reduce the number of gradient (Fock matrix) evaluations. The solver optimizes orthogonal orbitals by sequences of unitary rotations generated by the (preconditioned) limited-memory Broyden-Fletcher-Goldfarb-Shanno (L-BFGS) algorithm incorporating trust-region step restriction. Low-rank structure of the inverse (approximate) Hessian is exploited not only in L-BFGS but also when solving the trust-region problem. The efficiency of the proposed “Quasi-Newton Unitary Optimization with Trust-Region” (QUOTR) method is compared to that of the standard Roothaan-Hall approach accelerated by the Direct Inversion of Iterative Subspace (DIIS), and other exact and approximate Newton solvers for mean-field (Hartree-Fock and Kohn-Sham) problems.

## 1 Introduction

Orbital optimization via self-consistent field (SCF) is a fundamental ingredient of the electronic structure methods at all levels of approximation, from 1-body models (Hartree-Fock

(HF), Kohn-Sham Density Functional Theory (KS-DFT)) to many-body methods (multiconfiguration self-consistent field (MCSCF)). Despite the long history of innovation,<sup>1-28</sup> efforts to develop improved SCF solvers continue to this day,<sup>29-33</sup> driven by the desire to reduce computational cost and to improve robustness. Most popular solvers in the molecular context are based on the Roothaan-Hall (RH) iterative diagonalization of the Fock matrix<sup>1,34</sup> augmented by convergence accelerators such as Anderson mixing<sup>35</sup> known in chemistry as direct inversion in the iterative subspace (DIIS),<sup>9,12</sup> as well as others.<sup>36</sup> However, several issues plague the efficient RH/DIIS heuristics:

- for systems with complex electronic structure (such as molecules far from equilibrium, open-shell systems,<sup>31,37</sup> and systems with small HOMO-LUMO gaps<sup>27</sup>) convergence will be slow,<sup>38</sup> erratic, or nonexistent,<sup>30,39</sup>
- the use of diagonalization produces canonical orbitals whose lack of localization makes the use of orbital-based reduced-scaling formalisms for Fock matrix construction difficult,
- applications to large systems and/or in non-LCAO representations can be bottlenecked by the  $\mathcal{O}(N^3)$  cost of diagonalization,<sup>16,17,25</sup>
- locating non-Aufbau (e.g., excited state) solutions is possible<sup>40</sup> but is not robust, and
- even in favorable cases the convergence rate is linear<sup>41,42</sup> (i.e. error reduced by approximately the same factor each iteration) even in the vicinity of the solution; this is slower than the quadratic convergence exhibited by, e.g., the Newton method.<sup>43</sup>

SCF solvers relying on the direct energy minimization can address some/all of these concerns and thus have a long history of development.<sup>2,4,5,7,8,10,11,13-18,20-28,44</sup> In the molecular context direct minimization mean-field SCF solvers have long been employed as the recommended alternative in the case of convergence problems, used in combination with the RH/DIIS to gain superlinear convergence, and to enable reduced-scaling SCF approaches<sup>25,27</sup>

Nevertheless, RH/DIIS remains the default SCF solver in most quantum chemistry packages. Clearly, this is not due to its formal advantages, but due to its superior efficiency. This may be puzzling, since direct minimization solvers are often demonstrated to converge in as few as (or fewer) *iterations* than RH/DIIS. However, the number of iterations is a misleading figure since each update of the orbitals or density matrix may involve multiple energy/gradient evaluations or solving similarly-expensive subproblems (such as multiplication by the orbital Hessian). In other words, the number of Fock matrix builds ( $N_F$ ) in a direct minimization solver is typically significantly greater than the number of iterations ( $N_I$ ), whereas in RH/DIIS they are equal. Thus the latter typically involves significantly fewer Fock matrix evaluations, which in most practical applications determines the overall cost of SCF.

The objective of this work is to develop a reduced-scaling direct minimization SCF solver that obtains as low a cost as possible, namely by reducing the number of Fock matrix evaluations and avoiding the need for exact Hessian evaluation. The resulting “Quasi-Newton Unitary Optimization with Trust-Region” (QUOTR) SCF solver uses preconditioned limited-memory Broyden–Fletcher–Goldfarb–Shanno (L-BFGS) algorithm<sup>43</sup> step-restricted by trust-region (TR) and leverages the inverse BFGS Hessian’s low-rank structure to efficiently solve the trust-region update problem.<sup>45</sup>

The rest of the manuscript is structured as follows. In Section 2 we briefly review the general classes of SCF solvers before describing the theoretical aspects of QUOTR. Next, the implementation of QUOTR is discussed in Section 3. In Section 4 we display solver performance statistics for a standard set of chemical systems and make comparison to a method that uses “exact Hessian”. Additionally, in Section 4 we illustrate its utility for a problem where the RH/DIIS solver could not find a solution, namely a simple neuropeptide containing 75 atoms from Ref. 39. In Section 5 we summarize our findings and offer suggestions for further improvement.

## 2 Formalism

### 2.1 Overview of SCF Solver Approaches

All SCF methods attempt to iteratively minimize the variational energy  $E(\mathbf{x})$ , where  $\mathbf{x}$  is a set of independent parameters defining the particular method. In practice the minimum is determined by using the energy, its gradient  $\mathbf{g}$ , and optionally the Hessian  $\mathbf{B}$ . Starting with an initial (guess) set of parameters  $\mathbf{x}^{(0)}$  SCF constructs improved parameter values using the current energy and its derivatives, (optionally) their values from previous iterations (histories), as well as any optional additional parameters and their histories:

$$\mathbf{x}^{(k+1)} = f(\{\mathbf{x}^{(k)}\}, \{E^{(k)}\}, \{\mathbf{g}^{(k)}\}, \dots) \quad (1)$$

The SCF solvers differ in how they construct the update in Eq. (1); unfortunately it is not possible to systematically classify the solvers since in the vast majority of cases  $f()$  is an algorithm, not a simple function. Thus here we only focus on essential common elements of all SCF solvers.

Most solvers split the update problem (1) into 2 subproblems by defining the parameter update,

$$\mathbf{s}^{(k)} \equiv \mathbf{x}^{(k+1)} - \mathbf{x}^{(k)} = \alpha^{(k)} \mathbf{p}^{(k)} \quad (2)$$

in terms of a search direction  $\mathbf{p}^{(k)}$  and a step size  $\alpha^{(k)}$ , each of which has its own prescription similar to Eq. (1)

$$\mathbf{p}^{(k)} = g(\{\mathbf{x}^{(k)}\}, \{E^{(k)}\}, \{\mathbf{g}^{(k)}\}, \dots), \quad (3)$$

$$\alpha^{(k)} = h(\{\mathbf{x}^{(k)}\}, \{E^{(k)}\}, \{\mathbf{g}^{(k)}\}, \dots). \quad (4)$$

The need to control the step size is common to all SCF solvers due to the fundamental

nonlinearity of the energy function. Therefore even solvers that do not employ Eq. (2), such as RH/DIIS, still introduce ad hoc ways to control the step size by level shifting, damping, and other means of step restriction.

The simplest “2-step” solver is the steepest descent (SD) method<sup>2</sup> in which the search direction  $\mathbf{p}^{(k)}$  is opposite to the current gradient  $\mathbf{g}^{(k)}$ :

$$\mathbf{p}^{(k)} \stackrel{\text{SD}}{\equiv} - \frac{\mathbf{g}^{(k)}}{\|\mathbf{g}^{(k)}\|} \quad (5)$$

Unfortunately, although SD method is guaranteed to converge to a nearby minimum, the plain SD variant converges very slowly;<sup>46,47</sup> this can be rationalized by comparing it to the (exact) Newton step:

$$\mathbf{s}^{(k)} \stackrel{\text{Newton}}{\equiv} - (\mathbf{B}^{(k)})^{-1} \mathbf{g}^{(k)}. \quad (6)$$

Hessian  $\mathbf{B}$  is a diagonally-dominant matrix with large (and growing with the basis set size) condition number. Luckily it is relatively simple to construct an effective approximation to the Hessian; a particularly popular way is to use only the 1-electron terms in the Hessian,  $\mathbf{B}_{1e}$ . Approximate Hessians can then be used for preconditioning SD (using the 1-electron Hessian for preconditioning is also known as the “energy weighted steepest descent” method<sup>4,5,7</sup>) by replacing  $\mathbf{g}^{(k)}$  in Eq. (5) with the preconditioned gradient:

$$\bar{\mathbf{g}}^{(k)} \equiv (\mathbf{B}_{1e}^{(k)})^{-1} \mathbf{g}^{(k)}. \quad (7)$$

The RH method can be viewed as a simplified version of preconditioned SD, due to its step being exactly the negative of the gradient preconditioned by the 1-electron Hessian:<sup>23,27</sup>

$$\mathbf{s}^{(k)} \stackrel{\text{RH}}{\equiv} - \bar{\mathbf{g}}^{(k)}. \quad (8)$$

More sophisticated prescriptions for direction include the conjugate gradient (CG) method<sup>17,19,21,26,28</sup> in which history is limited to the information about the current and previous iteration. Of course, use of preconditioning is mandatory with CG just as with SD. Unfortunately neither SD nor CG, even with an approximate preconditioner, lead to optimal convergence rate near the minimum. Thus the most efficient solvers utilize exact or approximate Hessians near the minimum. Models that use the exact Hessian have been developed to avoid storage of the full Hessian, and rather calculate the Hessian-vector products at roughly the cost of a Fock build.<sup>12,15,16</sup> Although it is possible to apply straightforward Newton method using exact Hessian when sufficiently close to the minimum,<sup>8</sup> to be able to use exact Hessian further away from the minimum requires some form of step restriction. The popular augmented Hessian (AH)<sup>30</sup> method can be viewed as a Newton method with optimally restricted step, it can also be viewed as a quasi-Newton method in which approximate (level-shifted) Hessian is used. The diverse family of quasi-Newton methods use approximate Hessians of some form, often generated from information contained in the gradients and steps of the previous iterations.<sup>43</sup> The quasi-Newton idea has been used in MCSCF for a long time,<sup>48</sup> and the most commonly employed approximation in SCF is some form of the Broyden-Fletcher-Goldfarb-Shanno (BFGS) algorithm.<sup>13,14,18,20,28,32</sup>

Although some solvers compute step length separately from direction more sophisticated approaches fuse step restriction more deeply into the step computation. Indeed, when an underlying quadratic model of the energy exists, it is not natural to simply perform a line search toward the (unrestricted) minimum of the model, considering that the model is known to be locally accurate in all directions. The alternative concept of searching for the minimum of a model in all directions, but restricting the step size to some maximum value, is the key idea of the trust-region (TR) methods.<sup>22-25,27,30,44,49,50</sup> Two important aspects of any TR method are: how the trust-region is updated between iterations, and how the trust-region problem is solved for the step. The update method that is commonly used is based on an algorithm developed by Fletcher,<sup>51</sup> and one of the first true TR applications to use this in

quantum chemistry was implemented for MCSCF theory.<sup>49</sup> A common way to solve the TR problem in quantum chemistry is within the framework of the AH method.<sup>30</sup> This has the benefit of properly dealing with negative eigenvalues in the Hessian, and is thus often used with full-Newton methods where the true Hessian can have negative eigenvalues away from the energy-minimizing solution. However, it is not the only way to solve the TR problem, and we have chosen to use a method from the mathematics literature that uses the low-rank structure of the L-BFGS Hessian to our advantage.<sup>45</sup>

## 2.2 QUOTR: Quasi-Newton Unitary Optimization with Trust Region

Our direct minimization SCF solver is a preconditioned quasi-Newton (L-BFGS) solver with step restriction applied using the trust-region (TR) method. Although its aspects are similar to prior SCF solvers, there are several novel elements:

- The optimization is parameterized with a consistent “reference” (epoch) MO basis allowing use of the exact gradient with minimal computation after the Fock matrix is built.
- The preconditioner is updated only on some iterations, and it is regularized in a simple way to ensure a positive definite Hessian.
- The low-rank structure of the L-BFGS Hessian is exploited when solving for the quasi-Newton step on the TR boundary.

The overall structure of QUOTR is presented in Algorithm 1. Below we elaborate on each key aspect of the solver.

### 2.2.1 Parameterization

It is important to consider how the standard unconstrained quasi-Newton minimization scheme can be mapped to the constrained minimization of the single-determinant energy

---

**Algorithm 1** QUOTR SCF Solver
 

---

```

 $S_{\text{updated}} \leftarrow \text{true}, k \leftarrow 0, \mathbf{v}_{\text{hist}} \leftarrow \{\}, R_{\text{hist}} \leftarrow \text{false}$ 
while ( $\|\mathbf{g}^{(k)}\|/n^2 > t_c$  AND  $\Delta E^{(k)} > t_c$ ) do
  if ( $S_{\text{updated}} = \text{true}$ ) then
     $\bar{\mathbf{g}}^{(k)} \leftarrow (\mathbf{B}_{1e}^{-1/2}) n_s [\mathbf{F}_{\text{epoch}}^{(k)}, \mathbf{P}_{\text{epoch}}^{(k)}]$ 
    if ( $k > 0$  AND  $\bar{\mathbf{y}}^{(k-1)} \cdot \tilde{\mathbf{s}}^{(k-1)} > t_r \|\mathbf{y}^{(k-1)}\| \|\mathbf{s}^{(k-1)}\|$ ) then
       $\mathbf{v}_{\text{hist}} \leftarrow \{\{\bar{\mathbf{y}}^{(k-1)}, \tilde{\mathbf{s}}^{(k-1)}\}, \mathbf{v}_{\text{hist}}\}$ 
    end if
  end if
  if ( $\Delta^{(k)} < t_t$  OR  $\mathbf{g}^{(k)}$  satisfies Eq. (41)) then  $R_{\text{hist}} \leftarrow \text{true}$ 
  if ( $R_{\text{hist}} = \text{false}$ ) then
    if ( $k > 0$  AND  $|\mathbf{v}_{\text{hist}}| > 0$ ) then
       $\tilde{\mathbf{s}}^{(k)} \leftarrow -(\tilde{\mathbf{H}}_{\text{BFGS}}^{(k)})\bar{\mathbf{g}}^{(k)}$ 
      if  $\|\tilde{\mathbf{s}}^{(k)}\| > \Delta^{(k)}$  then solve Eq. (36) for new  $\tilde{\mathbf{s}}^{(k)}$ 
      if ( $q^{(k)} > 0$ ) then  $R_{\text{hist}} \leftarrow \text{true}$ 
    else
       $\tilde{\mathbf{s}}^{(k)} \leftarrow -\bar{\mathbf{g}}^{(k)}$ 
    end if
  end if
  if ( $R_{\text{hist}} = \text{true}$ ) then
     $\mathbf{v}_{\text{hist}} \leftarrow \{\}, \mathbf{C}^{(r)} \leftarrow \mathbf{C}^{(k)}$ , pseudo-canonicalize  $\mathbf{F}^{(k)}$ , update  $\mathbf{B}_{1e}$ , recalculate  $\bar{\mathbf{g}}^{(k)}$ 
     $\mathbf{U}_{\text{epoch}}^{(k-1)} \leftarrow \mathbf{I}$ 
     $\tilde{\mathbf{s}}^{(k)} \leftarrow -\bar{\mathbf{g}}^{(k)}$ 
  end if
  if ( $k = 0$  OR  $|\mathbf{v}_{\text{hist}}| = 0$ ) then do line search for new step:  $\tilde{\mathbf{s}}^{(k)} \leftarrow \alpha^{(k)}\tilde{\mathbf{s}}^{(k)}/\|\tilde{\mathbf{s}}^{(k)}\|$ 
   $\mathbf{C}^{(k+1)} \leftarrow \mathbf{C}^{(r)}\mathbf{U}_{\text{epoch}}^{(k)}$ , build  $\mathbf{F}_{\text{AO}}^{(k+1)}$ , and  $\Delta E^{(k)} \leftarrow E^{(k+1)} - E^{(k)}$ 
  if ( $k > 0$  AND  $|\mathbf{v}_{\text{hist}}| > 0$ ) then
     $\rho^{(k)} \leftarrow \Delta E^{(k)}/q^{(k)}$ 
    if  $\rho^{(k)} < \tau_1$  then
      reject step: reset to  $\mathbf{C}^{(k)}$ ,  $\mathbf{U}_{\text{epoch}}^{(k)}$ ,  $\mathbf{F}_{\text{AO}}^{(k)}$ ,  $\mathbf{P}_{\text{epoch}}^{(k)}$ ,  $S_{\text{updated}} \leftarrow \text{false}$ 
    else
      accept step:  $S_{\text{updated}} \leftarrow \text{true}, k \leftarrow k + 1$ 
    end if
  if  $\rho^{(k)} < \tau_2$  then
     $\Delta^{(k)} \leftarrow \min(\eta_1 \Delta^{(k)}, \eta_2 \|\tilde{\mathbf{s}}^{(k)}\|)$ 
  else if ( $\rho^{(k)} > \tau_3$  AND  $\|\tilde{\mathbf{s}}^{(k)}\| > \eta_3 \Delta^{(k)}$ ) then
     $\Delta^{(k)} \leftarrow \eta_4 \Delta^{(k)}$ 
  end if
else
  if  $\Delta E^{(k)} > 0$  then
    reject step: reset  $\mathbf{C}^{(k)}$ ,  $\mathbf{U}_{\text{epoch}}^{(k)}$ ,  $\mathbf{F}_{\text{AO}}^{(k)}$ ,  $\mathbf{P}_{\text{epoch}}^{(k)}$ ,  $S_{\text{updated}} \leftarrow \text{false}$ 
  else
    accept step:  $S_{\text{updated}} \leftarrow \text{true}, k \leftarrow k + 1$ , and  $\Delta^{(k)} \leftarrow \|\tilde{\mathbf{s}}^{(k)}\|$ 
  end if
end if
end while

```



where the orbitals are required to be orthonormal. In the following we assume the linear combination of atomic orbitals (LCAO) representation of the molecular orbitals (MOs), and thus the MOs are defined by the coefficient matrix  $\mathbf{C}$ .

We seek a unitary matrix,  $\mathbf{U}_{\text{total}}$ , that transforms a set of orthonormal orbitals,  $\mathbf{C}^{(0)}$ , into the energy minimizing solution,  $\mathbf{C}_{\text{min}}$ .

$$\mathbf{C}_{\text{min}} = \mathbf{C}^{(0)}\mathbf{U}_{\text{total}} \quad (9)$$

We iteratively build the total unitary matrix as a product of individual unitary matrices generated at each iteration, indexed by  $k$  in Eq. (10).

$$\mathbf{U}_{\text{total}} = \prod_k \mathbf{U}^{(k)} \quad (10)$$

At the start of iteration  $k$  the total unitary matrix is composed of a product of only the first  $k$  individual unitary matrices, the others not yet determined. During iteration  $k$  the new total unitary matrix is determined by finding  $\mathbf{U}^{(k)}$  and then multiplying it with the growing product.

$$\mathbf{U}_{\text{total}}^{(k)} = \prod_{p=0}^{p=k} \mathbf{U}^{(p)} \quad (11)$$

Similarly, the MOs at the start of iteration  $k > 0$  are given by the coefficient matrix obtained from the total rotation determined thus far.

$$\mathbf{C}^{(k)} = \mathbf{C}^{(0)}\mathbf{U}_{\text{total}}^{(k-1)} \quad (12)$$

Thus, the next set of MOs is determined by rotating the previous set of orbitals.

$$\mathbf{C}^{(k+1)} = \mathbf{C}^{(k)}\mathbf{U}^{(k)} = \mathbf{C}^{(0)}\mathbf{U}_{\text{total}}^{(k)} \quad (13)$$

This formulation, where the orbitals are “reset” each iteration, has been used many times before,<sup>8,18,20,52</sup> and it is helpful for simplifying the calculation of the gradient, as will be described shortly.

We use the exponential parameterization of unitary rotations, common in electronic structure theory,<sup>8,53–55</sup> which allows us to work with the independent elements of an antihermitian matrix,  $\boldsymbol{\kappa}$ , without any restrictions on the values of these components, and thereby maintain orthonormal MOs. At iteration  $k$  we determine a unitary rotation by finding  $\boldsymbol{\kappa}^{(k)} = -(\boldsymbol{\kappa}^{(k)})^T$  using a prescription described later. We then update the orbitals by applying the unitary rotation defined by  $\boldsymbol{\kappa}^{(k)}$  through Eq. (14) to the growing  $\mathbf{U}_{\text{total}}$ .

$$\mathbf{U}^{(k)} = \exp(\boldsymbol{\kappa}^{(k)}) \tag{14}$$

The matrix exponentials are evaluated accurately with a Taylor series expansion using a tight convergence threshold, so that no later reorthogonalization is necessary, in contrast to some methods.<sup>8,18</sup> The simple scaling-and-squaring approach with a fixed order of 2 is used.<sup>30,56</sup> Thus, the elements of the step vector are divided by  $2^2 = 4$  before performing the Taylor series expansion, and the resulting converged unitary matrix is squared twice. Although the matrix exponential could be improved further, e.g., by leveraging the block-sparse antihermitian structure of  $\boldsymbol{\kappa}$ ,<sup>33</sup> our focus is on the overall SCF method and its cost in terms of  $N_{\text{F}}$ . What is important to note about the matrix exponentials in our implementation is that they are computed nearly exactly (to within a tolerance,  $t_e$ ) so that no reorthogonalization is needed. This is important because we need to know how the independent parameters change in each iteration to be able to form the quasi-Newton approximation to the Hessian.

It is important to express both the gradients and steps in the same basis between iterations when using a quasi-Newton approximation for the Hessian, since the standard update formulas assume a fixed basis. It is well known that the gradient of the energy with respect

to the matrix elements of  $\boldsymbol{\kappa}$  is easily found from the MO Fock matrix:

$$\frac{\partial E}{\partial \boldsymbol{\kappa}_{ai}^{(k)}} = n_s \mathbf{F}_{ai}^{(k)}, \quad (15)$$

where  $a$  and  $i$  refer to the unoccupied and occupied MOs, respectively, and  $n_s$  is twice the occupancy of orbitals  $i$  (4 for spin restricted wavefunctions, 2 for spin unrestricted wavefunctions). This expression holds because  $\mathbf{U}^{(k)}$  is rotating the current orbitals, as in Eq. (13), so that the gradient is composed of partial derivatives evaluated for  $\boldsymbol{\kappa}^{(k)} = \mathbf{0}$  in Eq. (14). After the MOs are rotated, the MO basis is changed so that the indices  $a$  and  $i$  on the MO Fock matrix in Eq. (15) refer to different orbitals for iterations  $k$  and  $k + 1$ . Therefore, we cannot use this formula for the history gradients when constructing the L-BFGS Hessian. To avoid this problem we always compute the gradient in the same ‘‘reference’’ MO basis for the given sequence of iterations comprising the history *epoch*; the reference basis can only be changed (e.g., when updating the preconditioner, see Section 2.2.2) in combination with resetting of the history. This epoch MO basis for iteration  $k$  is simply the initial set of MOs,  $\mathbf{C}^{(r)}$ , at the start of the epoch. MO basis  $\mathbf{C}^{(k)}$  for iteration  $k \geq r$  is related to the epoch MO basis  $\mathbf{C}^{(r)}$  by the unitary obtained as a product of each interstitial iterations’ update:

$$\mathbf{C}^{(k)} = \mathbf{C}^{(r)} \mathbf{U}_{\text{epoch}}^{(k-1)} \equiv \mathbf{C}^{(r)} \mathbf{U}^{(r)} \mathbf{U}^{(r+1)} \dots \mathbf{U}^{(k-1)} \quad (16)$$

This formalism simplifies the calculation of the gradient,  $\mathbf{g}^{(k)}$ , in the epoch basis, as shown in Eq. (17).

$$\mathbf{g}^{(k)} \equiv n_s [\mathbf{F}_{\text{epoch}}^{(k)}, \mathbf{P}_{\text{epoch}}^{(k)}] \quad (17)$$

Here  $\mathbf{F}_{\text{epoch}}^{(k)}$  is the Fock matrix expressed in the epoch MO basis and  $\mathbf{P}_{\text{epoch}}^{(k)}$  is a projector onto the occupied space. The Fock matrix is evaluated in AO basis using the current iteration’s

occupied MOs and then transformed to the epoch basis:

$$\mathbf{F}_{\text{epoch}}^{(k)} = (\mathbf{C}^{(r)})^T \mathbf{F}_{\text{AO}}^{(k)} \mathbf{C}^{(r)} \quad (18)$$

The projection operator onto the occupied space at iteration  $k$  in the epoch basis is obtained as

$$\mathbf{P}_{\text{epoch}}^{(k)} = \mathbf{U}_{\text{epoch}}^{(k)} \mathbf{P} (\mathbf{U}_{\text{epoch}}^{(k)})^T, \quad (19)$$

where  $\mathbf{P} = \text{diag}(\{n_i\})$  and  $n_i$  is the occupancy of spin orbital  $i$ . It should be noted that  $n_s$  in Eq. (17) accounts for double/single occupancy of orbitals. For spin unrestricted orbitals we rotate the alpha and beta coefficient matrices separately, and thus there is a separate gradient, projector and Fock matrix for each. This is why  $n_i$  in the construction of  $\mathbf{P}$  is always either 0 or 1, even for the spin restricted case; hence,  $\mathbf{P}$  is a projector. Not only does this formulation of the gradient allow us to have a consistent basis for forming the L-BFGS Hessian, it also avoids a non-truncating series expression for the gradient, as in other solvers.<sup>32</sup>

While  $\boldsymbol{\kappa}$  is indeed a matrix, and it is necessary to be able to find its matrix exponential to calculate  $\mathbf{U}$ , we will generally work with a vector of the independent elements as the parameters for determining a step in iteration  $k$ . We obtain a vector space with no constraints on the value of the vector components if we use only the upper (or lower) triangle of the kappa matrix (the other elements being determined by the antihermitian requirement:  $\boldsymbol{\kappa}_{pq} = -\boldsymbol{\kappa}_{qp}$ ). This vector space will be called  *$\boldsymbol{\kappa}$ -space* throughout this manuscript. We only consider real values for  $\boldsymbol{\kappa}_{pq}$ , and so the diagonal elements must be zero. For an MO basis with  $n$  orbitals, this means that the  *$\boldsymbol{\kappa}$ -space* has dimension  $n(n - 1)/2$ , assuming no symmetry is taken into account. The independent elements of the kappa matrix are collected into a single vector, which we refer to as a *step*,  $\mathbf{s}$ . In the spin unrestricted case, the kappa elements for the separate alpha and beta spin MOs are simply concatenated into one large vector.

Considering the antisymmetry produced by the commutator in Eq. (17), the gradient is properly a member of the  $\kappa$ -space. Thus, we can map the matrix elements of the gradient to a vector in exactly the same way as for the matrix elements of  $\kappa$ , using only the upper (or lower) triangle. We use the symbol  $\mathbf{s}^{(k)}$  for the vector version of  $\kappa^{(k)}$ , but make no such distinction for the gradient,  $\mathbf{g}^{(k)}$ : the use should be clear from context.

The steps and gradient differences are the ingredients for the L-BFGS update to the Hessian. Thus, when these history vectors are saved, we keep them both in the epoch MO basis. There is never a need to transform the gradients to the current MO basis, only the steps are transformed. Every time a step is calculated using L-BFGS, the algorithm is performed in the epoch MO basis. Then, it is transformed to the *current* MO basis of iteration  $k$  before taking the exponential and multiplying it by the growing total unitary rotation. We can then write  $\kappa^{(k)} = \mathbf{U}_{\text{epoch}}^{(k-1)\text{T}} \kappa_{\text{epoch}}^{(k)} \mathbf{U}_{\text{epoch}}^{(k-1)}$  as how we can obtain useful parameters that were found in the epoch MO basis. Thus, we can revise Eq. (14) to combine the basis transformation with the exponentiation.

$$\mathbf{U}^{(k)} = \exp(\mathbf{U}_{\text{epoch}}^{(k-1)\text{T}} \kappa_{\text{epoch}}^{(k)} \mathbf{U}_{\text{epoch}}^{(k-1)}) \quad (20)$$

The convergence criteria are that both the gradient norm per element,  $\|\mathbf{g}^{(k)}\|/n^2$ , and the energy difference between iterations,  $\Delta E^{(k)}$ , are lower than a threshold  $t_c$ . However, for some comparisons with other solvers, we use the gradient norm (of the gradient as a matrix) instead of the per element version.

### 2.2.2 Quasi-Newton

The L-BFGS algorithm is used to approximate the Hessian,  $\mathbf{B}_{\text{BFGS}}^{(k)} \approx \mathbf{B}^{(k)}$ , and its inverse,  $\mathbf{H}_{\text{BFGS}}^{(k)} \equiv (\mathbf{B}_{\text{BFGS}}^{(k)})^{-1} \approx (\mathbf{B}^{(k)})^{-1}$ , using the “history” vectors from (at most)  $m$  previous iterations. In the following we will assume that the history size is equal to  $m$  for simplicity.

This approximate Hessian and its inverse can be represented in low-rank form as follows:<sup>45</sup>

$$\mathbf{B}_{\text{BFGS}}^{(k)} = \mathbf{B}_0 - \mathbf{V}_B^{(k)}(\mathbf{W}^{(k)})^{-1}\mathbf{V}_B^{(k)\text{T}} \quad (21)$$

$$\mathbf{H}_{\text{BFGS}}^{(k)} = \mathbf{H}_0 + \mathbf{V}_H^{(k)}\mathbf{M}^{(k)}\mathbf{V}_H^{(k)\text{T}} \quad (22)$$

Here the matrix  $\mathbf{B}_0$  is an initial (often diagonal) approximation to the Hessian, which in principle could be any positive definite matrix.<sup>43</sup> The matrix  $\mathbf{H}_0$  is the corresponding initial inverse Hessian approximation:  $\mathbf{H}_0 = (\mathbf{B}_0)^{-1}$ . More will be said about these critical components later. The matrix  $\mathbf{V}_B^{(k)}$  is composed of columns of the  $m$  previous steps multiplied by the initial Hessian,  $\mathbf{B}_0\mathbf{s}^{(k)}$ , followed by  $m$  columns of previous gradient differences,  $\mathbf{y}^{(k)} \equiv \mathbf{g}^{(k+1)} - \mathbf{g}^{(k)}$ , and therefore has dimension  $n \times 2m$ . Similarly,  $\mathbf{V}_H^{(k)}$  contains the same information, but in a slightly different form:  $\mathbf{V}_H^{(k)} = \mathbf{H}_0\mathbf{V}_B^{(k)}$ . The square matrices  $\mathbf{W}^{(k)}$  and  $\mathbf{M}^{(k)}$  have dimension  $2m \times 2m$ , and the need for the inverse of  $\mathbf{W}^{(k)}$  is not a problem since  $m$  is typically small (less than 20). The formation of  $\mathbf{W}^{(k)}$  and  $\mathbf{M}^{(k)}$  is described in the literature,<sup>45,57</sup> but essentially they are composed of various dot products involving the history vectors, with an inverse of one of the  $m \times m$  subblocks.

$$\mathbf{W}^{(k)} = \left( \begin{array}{c|c} ((\mathbf{S}^{(k)})^{\text{T}}\mathbf{B}_0\mathbf{S}^{(k)}) & \mathbf{L}^{(k)} \\ \hline (\mathbf{L}^{(k)})^{\text{T}} & -\mathbf{E}^{(k)} \end{array} \right) \quad (23)$$

$$\mathbf{M}^{(k)} = \left( \begin{array}{c|c} ((\mathbf{L}^{(k)})^{-1}(\mathbf{E}^{(k)} + (\mathbf{Y}^{(k)})^{\text{T}}\mathbf{H}_0\mathbf{Y}^{(k)})(\mathbf{L}^{(k)})^{-\text{T}}) & -(\mathbf{L}^{(k)})^{-1} \\ \hline -(\mathbf{L}^{(k)})^{-\text{T}} & 0 \end{array} \right) \quad (24)$$

In Eq. (23) and Eq. (24),  $\mathbf{S}^{(k)}$  is an  $n \times m$  matrix containing the history column vectors of the  $\mathbf{s}^{(k)}$ , and  $\mathbf{Y}^{(k)}$  similarly contains  $\mathbf{y}^{(k)}$ . The smaller  $m \times m$  sub matrices  $\mathbf{L}^{(k)}$  and  $\mathbf{E}^{(k)}$

are simply constructed as below.

$$\mathbf{L}_{ij} = \begin{cases} \mathbf{s}^{(k-m-1+i)} \cdot \mathbf{y}^{(k-m-1+j)}, & \text{if } i > j \\ 0 & \text{otherwise} \end{cases} \quad (25)$$

$$\mathbf{E}_{ij} = \begin{cases} \mathbf{s}^{(k-m-1+i)} \cdot \mathbf{y}^{(k-m-1+j)} & \text{if } i = j \\ 0 & \text{else} \end{cases} \quad (26)$$

One of the advantages of the L-BFGS Hessian approximation, apart from not requiring calculation of second derivatives, is that it can be stored in this factorized form by simply keeping the relatively small matrices  $\mathbf{B}_0$ ,  $\mathbf{V}_B^{(k)}$ , and  $\mathbf{W}^{(k)}$ . Considering that  $\mathbf{B}_0$  is a diagonal matrix, we only need to store  $(2m + 1)n + 4m^2$  elements, which is typically much smaller than the full Hessian which requires  $n^2$  elements. From the development up to this point it would seem that we also need to store the information for the inverse L-BFGS Hessian, specifically  $\mathbf{V}_H^{(k)}$ , but this will be dealt with soon.

The quasi-Newton step,  $\mathbf{s}^{(k)} = -\mathbf{H}_{\text{BFGS}}^{(k)}\mathbf{g}^{(k)}$ , is calculated by multiplying the inverse L-BFGS Hessian of Eq. (22) with the negative of the gradient. Thus, the factorized form makes calculation of the quasi-Newton step simply a matter of a few matrix-vector multiplications. Note that although we only need the inverse Hessian to compute the quasi-Newton step, the Hessian is used to compute the energy decrease predicted by the quadratic model. This is needed for determining how the TR is updated between iterations as described in Section 2.2.3.

As is well known, the use of a physically relevant preconditioner is necessary to have convergence that is competitive with diagonalization methods.<sup>18,20</sup> A manifestation of a preconditioner is the choice of the initial diagonal Hessian ( $\mathbf{B}_0$ ). We construct this component using a formula requiring the MO Fock matrix that becomes equivalent to the 1-electron part

of the RHF Hessian as the regularizer goes to zero. Thus we call it  $\mathbf{B}_{1e}$ , since it comes from the 1-electron part.

$$(\mathbf{B}_{1e})_{(ia)(ia)} = n_s(\mathbf{F}_{aa} - \mathbf{F}_{ii} + r_{ia}) \quad (27)$$

The elements of the MO Fock matrix that are used in Eq. (27) are “pseudocanonical”,<sup>4</sup> meaning that the occupied-occupied block is diagonalized and the unoccupied-unoccupied block is diagonalized, but the off-diagonal occupied-unoccupied block is non-zero (unless at convergence). Therefore, to form this initial diagonal Hessian, we first apply a unitary rotation that does not change the energy, but mixes occ-occ and unocc-unocc to diagonalize each separately. The final term in Eq. (27),  $r_{ia}$ , is a regularization parameter that depends on the Fock matrix elements and ensures that the diagonal Hessian is positive definite.

$$r_{ia} = \begin{cases} t_r + \mathbf{F}_{ii} - \mathbf{F}_{aa} & \text{if } :(\mathbf{F}_{aa} - \mathbf{F}_{ii}) < t_r \\ 0 & \text{else} \end{cases} \quad (28)$$

In Eq. (28)  $t_r$  is a threshold for the minimum value for the difference in “pseudocanonical” orbital energies  $\mathbf{F}_{aa}$  and  $\mathbf{F}_{ii}$ . Unlike some other quasi-Newton solvers,<sup>20</sup> we do not update the diagonal part of the approximate Hessian every iteration. In principle this could lead to slower convergence, since the approximation degrades as the orbitals are changed from the point where the diagonal Hessian was calculated. Indeed, we found that in the early iterations it is imperative to use an updated preconditioner, and thus we do an approximate line search along the preconditioned steepest descent direction until the max element of the gradient drops below some threshold (we use 0.1 which is smaller than 0.25, which has literature precedent<sup>18</sup>). During this early phase of the solver, the orbitals are made “pseudocanonical” each iteration, and the preconditioner is rebuilt. Essentially, the epochs are only 1 iteration long. However, near the solution, we have found that it is not necessary to update the preconditioner every iteration, and because we work in the epoch MO basis



it would be difficult to update the preconditioner. We have found that with a good initial guess, only a median of 2 iterations of this line search are required to drop the max gradient element below 0.1 and trigger L-BFGS starting for simple systems (see Section 4.1). If the gradient gets large again, the history is reset and preconditioned steepest descent is again carried out with an updated preconditioner. Every time the history is reset the epoch basis is also reset to the current orbitals.

An alternative and perhaps more conventional view of the preconditioner is that it is a basis transformation that makes the diagonal part of the L-BFGS Hessian or its inverse closer to an identity matrix. To see how this view relates to the diagonal Hessian, consider the following transformation of the quasi-Newton equation:  $\mathbf{s} = -(\mathbf{H}_{\text{BFGS}})\mathbf{g}$  (omitting iteration index). Multiply both sides of the equation by  $\mathbf{B}_{1e}^{1/2}$  and insert the identity  $\mathbf{I} = \mathbf{B}_{1e}^{1/2}\mathbf{B}_{1e}^{-1/2}$  (which is clearly acceptable because the diagonal matrix  $\mathbf{B}_{1e}$  is guaranteed to be positive definite due to the regularizer) between the inverse Hessian and the gradient, to get an equivalent equation.

$$\mathbf{B}_{1e}^{1/2}\mathbf{s} = -(\mathbf{B}_{1e}^{1/2}\mathbf{H}_{\text{BFGS}}\mathbf{B}_{1e}^{1/2})\mathbf{B}_{1e}^{-1/2}\mathbf{g} \quad (29)$$

Setting  $\tilde{\mathbf{s}} = \mathbf{B}_{1e}^{1/2}\mathbf{s}$ , we see that we are finding the quasi-Newton step with the modified gradient,  $\tilde{\mathbf{g}} = \mathbf{B}_{1e}^{-1/2}\mathbf{g}$ , and inverse Hessian,  $\tilde{\mathbf{H}}_{\text{BFGS}} = \mathbf{B}_{1e}^{1/2}\mathbf{H}_{\text{BFGS}}\mathbf{B}_{1e}^{1/2}$  to produce the modified step,  $\tilde{\mathbf{s}}$ . Considering the form of the L-BFGS inverse Hessian that we are using, the modified inverse Hessian reduces to the following.

$$\tilde{\mathbf{H}}_{\text{BFGS}} = \mathbf{B}_{1e}^{1/2}\mathbf{H}_{\text{BFGS}}\mathbf{B}_{1e}^{1/2} \quad (30)$$

$$= \mathbf{B}_{1e}^{1/2}(\mathbf{B}_{1e}^{-1} + \mathbf{V}_H\mathbf{M}(\mathbf{V}_H)^T)\mathbf{B}_{1e}^{1/2} \quad (31)$$

$$= (\mathbf{B}_{1e}^{1/2}\mathbf{B}_{1e}^{-1}\mathbf{B}_{1e}^{1/2}) + \mathbf{B}_{1e}^{-1/2}(\mathbf{V}_H\mathbf{M}(\mathbf{V}_H)^T)\mathbf{B}_{1e}^{-1/2} \quad (32)$$

$$= \mathbf{I} + \tilde{\mathbf{V}}\mathbf{M}\tilde{\mathbf{V}}^T \quad (33)$$

Where  $\tilde{\mathbf{V}} = \mathbf{B}_{1e}^{1/2} \mathbf{V}_H$ . Notice that we also have  $\tilde{\mathbf{V}} = \mathbf{B}_{1e}^{-1/2} \mathbf{V}_B$ . This provides a more unified way to form the L-BFGS Hessian and its inverse. If we work with the preconditioned quantities  $\tilde{\mathbf{s}}^{(k)}$  and  $\tilde{\mathbf{g}}^{(k)}$  we can form  $\tilde{\mathbf{V}}^{(k)}$  directly from them. Additionally, we do not have separate versions of the history for the Hessian and the inverse Hessian. The price that we pay is that we need to convert back to the “un-preconditioned” basis before taking the step. But this is simply a basis transformation:  $\mathbf{s}^{(k)} = \mathbf{B}_{1e}^{-1/2} \tilde{\mathbf{s}}^{(k)}$ . The preceding development of a preconditioned basis is essentially the “energy-weighted coordinates” previously introduced in the literature.<sup>13,20</sup> However, it should be emphasized that we do not update this basis every iteration.

Here is probably a good place to summarize the steps to obtain the unitary rotation at iteration  $k$ , since there are now quite a few layers.

$$\tilde{\mathbf{s}}^{(k)} \rightarrow \mathbf{s}^{(k)} \rightarrow \boldsymbol{\kappa}_{\text{epoch}}^{(k)} \rightarrow \boldsymbol{\kappa}^{(k)} \rightarrow \mathbf{U}^{(k)} \quad (34)$$

To keep the L-BFGS Hessian positive definite between iterations, we require the history vectors to satisfy the following.<sup>45</sup>

$$\tilde{\mathbf{s}}^{(k)} \cdot \bar{\mathbf{y}}^{(k)} > t_h \|\mathbf{s}^{(k)}\| \|\mathbf{y}^{(k)}\| \quad (35)$$

When this requirement is not met the pair of history vectors  $\{\tilde{\mathbf{s}}^{(k)}, \bar{\mathbf{y}}^{(k)}\}$  is not saved for future use. We have used  $t_h = 10^{-5}$ .

### 2.2.3 Trust-Region

Once the quasi-Newton step has been computed it is imperative for the robustness of the solver that we determine if the step is acceptable. Clearly, we want the energy to be lowered each iteration to prevent oscillations and non-convergence. Because the quadratic energy model may be inaccurate for large step sizes and because the L-BFGS Hessian is inherently an approximation for smaller  $m$ , restricting the step to a region where the model can be

“trusted” is a key way we achieve robustness. In the trust-region (TR) formalism we require the step to be within the trust-region.

$$\|\tilde{\mathbf{s}}^{(k)}\| \leq \Delta^{(k)} \quad (36)$$

In Eq. (36) the quantity  $\Delta^{(k)}$  is the trust-radius, which defines the trust-region. Notice first that the trust-radius is indexed by  $k$  so that it may differ between iterations. Fletcher’s algorithm,<sup>51</sup> which either expands or contracts the TR based on how accurate the model has been, is used to update the trust-radius (see Algorithm 1). We use parameters  $(\tau_i/\eta_i)$  from a more recent source.<sup>45</sup> The initial value of the trust-radius is set to the most recent successful line search step size since this should be in the correct order of magnitude for the next step. Also, we always do line search when there are no history data available so the most recent step size from line search is always a known quantity when quasi-Newton steps are attempted.

When the quasi-Newton step does not satisfy Eq. (36), we solve for the optimal step that is within the TR, which will be on the TR boundary:  $\|\tilde{\mathbf{s}}^{(k)}\| = \Delta^{(k)}$ . Our TR solver is based primarily on work from the mathematics literature that shows how to leverage the low-rank structure of the L-BFGS hessian.<sup>45</sup> The parameters for our implementation of the TR solver are given in Table 1, and the algorithm is given in Algorithm 2. In essence we iteratively update the parameter  $\sigma$ , which is a level-shift of the L-BFGS Hessian, until Eq. (36) is satisfied. We have made some modifications to improve stability and simplify when the TR is considered solved that appear to be sufficient for our purposes. One specific difference is that we do not use Cholesky decomposition to orthogonalize the columns of  $\tilde{\mathbf{V}}^{(k)}$ , but rather use matrix inverse square root:  $(\tilde{\mathbf{V}}^{(k)\text{T}}\tilde{\mathbf{V}}^{(k)})^{-1/2}$ .

Once a new step has been determined that satisfies the TR conditions, the energy change

Table 1: Parameters for TR solver

Description	Symbol	Value
Initial guess $\sigma$	$\sigma$	0.1
Convergence criterion 1	$T_1$	0.0001
Convergence criterion 2	$T_2$	$1 \times 10^{-7}$
maximum iterations	$i_{\max}$	500
sigma modify factor	$F_0$	1.1

expected from the quadratic model,  $q^{(k)}$ , is calculated according to the usual formula.

$$q^{(k)} = \tilde{\mathbf{s}}^{(k)} \cdot \tilde{\mathbf{g}}^{(k)} + \frac{1}{2} \tilde{\mathbf{s}}^{(k)} \cdot \tilde{\mathbf{B}}_{\text{BFGS}}^{(k)} \tilde{\mathbf{s}}^{(k)} \quad (37)$$

The new step is then tested by actually updating the coefficient matrix and constructing the associated Fock matrix. The step is then either accepted or rejected based on the actual energy change,  $\Delta E^{(k)}$ , if the step were to be taken. We have used the simple requirement that the actual energy change is not positive, and thus the energy will never increase between iterations. When the step is rejected, the trust-radius is decreased and a new TR problem is solved. Sometimes the TR may be shrunk repeatedly. The minimum allowed trust radius,  $t_t$ , is a way to detect if the quasi-Newton approximation is very bad. If for some reason the trust radius shrinks below this value, we reset the history, do a single line-search iteration, and continue from there.

Our source for the method of solving the TR problem using the low-rank structure of the L-BFGS Hessian assumes that the diagonal initial Hessian approximation is simply a scaled identity.<sup>45</sup> That is, the algorithm for solving the TR problem requires that the elements of the diagonal Hessian approximation be all the same. This would seem to preclude the use of any initial diagonal Hessian that is not a scaled identity, including the approximation based on the Fock matrix diagonal elements. However, if we work with the preconditioned quantities discussed in Section 2.2.2 the initial diagonal Hessian *is* the identity matrix in the epoch basis. Therefore, we can apply the method of solution presented in the literature source<sup>45</sup> to this modified TR problem, then transform back to the original basis before taking

---

**Algorithm 2** Trust-Region Solver

---

input:  $\mathbf{V}, \mathbf{W}^{-1}, \mathbf{g}, \delta, \Delta, \mathbf{s}_{\text{given}}$   
initialize:  $i_{\text{max}} \leftarrow 500, T_1 \leftarrow 1 \times 10^{-4}, T_2 \leftarrow 1 \times 10^{-7}, \sigma \leftarrow 0.1, C \leftarrow \text{false}$   
 $F, F_0 \leftarrow 1.1$   
 $\mathbf{R}^{1/2} = (\mathbf{V}^T \mathbf{V})^{1/2}$   
 $\mathbf{R}^{-1/2} = (\mathbf{V}^T \mathbf{V})^{-1/2}$   
diagonalize:  $(\mathbf{R}^{1/2})^T \mathbf{W}^{-1} \mathbf{R}^{1/2}$  to obtain eigenvectors as  $\mathbf{U}$  and eigenvalues as  $\Lambda$   
 $\mathbf{P}_{\parallel} = \mathbf{V} \mathbf{R}^{-1/2} \mathbf{U}$ , from Eq. 12 in Burdakov<sup>45</sup>  
 $\mathbf{g}_{\parallel} = (\mathbf{P}_{\parallel})^T \mathbf{g}$   
 $r_{\text{max}} = \dim(\mathbf{g}_{\parallel})$   
 $\|\mathbf{g}_{\perp}\|^2 = \|\mathbf{g}\|^2 - \|\mathbf{g}_{\parallel}\|^2$ , from Eq. 25 in Burdakov<sup>45</sup>  
 $i = 0$   
**while** not  $C$  AND  $i < i_{\text{max}}$  **do**  
     $\mathbf{v}_{\parallel} \leftarrow -(\Lambda + \sigma \mathbf{I})^{-1} \mathbf{g}_{\parallel}$ , from Eq. 16 in Burdakov<sup>45</sup>  
     $\|\mathbf{v}\| \leftarrow (\|\mathbf{v}_{\parallel}\|^2 + \|\mathbf{g}_{\perp}\|^2 / (\delta + \sigma)^2)^{1/2}$ , from Eq. 20 in Burdakov<sup>45</sup>  
     $v_{\text{temp}} \leftarrow -\|\mathbf{g}_{\perp}\|^2 / (\delta + \sigma)^3$ , from Eq. 21 in Burdakov<sup>45</sup>  
     $r \leftarrow 0$   
    **while**  $r < r_{\text{max}}$  **do**  
         $v_{\text{temp}} \leftarrow v_{\text{temp}} - (\mathbf{g}_{\parallel}[r])^2 / (\delta + \sigma)^3$ , from Eq. 21 in Burdakov<sup>45</sup>  
    **end while**  
     $\sigma \leftarrow \sigma - \frac{\phi(\sigma)}{\phi'(\sigma)} = \sigma - \frac{(\|\mathbf{v}\| - \Delta) \|\mathbf{v}\|^2}{\Delta v_{\text{temp}}}$ , from Eq. 19 in Burdakov<sup>45</sup>  
    **if**  $\sigma \in \{\sigma_{-1}, \sigma_{-2}, \sigma_{-3}, \sigma_{-4}\}$  **then**  
         $\sigma \leftarrow \frac{1}{2}(\sigma + \sigma_{-1})$   
    **end if**  
     $\{\sigma_{-1}, \sigma_{-2}, \sigma_{-3}, \sigma_{-4}\} \leftarrow \{\sigma, \sigma_{-1}, \sigma_{-2}, \sigma_{-3}\}$   
    **if**  $\|\|\mathbf{v}\| - \Delta\| \leq \min(T_1 \Delta, T_2)$  **then**  
        **if**  $\sigma < 0$  **then**  
             $\sigma \leftarrow -\sigma F$   
             $F \leftarrow F F_0$   
             $C = \text{false}$   
        **else if**  $\sigma \geq 0$  **then**  
             $C = \text{true}$   
        **end if**  
    **end if**  
     $i \leftarrow i + 1$   
**end while**  
 $\mathbf{v}_{\parallel} \leftarrow -(\Lambda + \sigma \mathbf{I})^{-1} \mathbf{g}_{\parallel}$ , from Eq. 16 in Burdakov<sup>45</sup>  
 $\mathbf{s} = \mathbf{P}_{\parallel}(\mathbf{v}_{\parallel} + (\delta + \sigma)^{-1} \mathbf{g}_{\parallel}) - (\delta + \sigma)^{-1} \mathbf{g}$ , from Eq. 27 in Burdakov<sup>45</sup>  
**if**  $i \geq i_{\text{max}}$  **then**  
     $\mathbf{s} \leftarrow \mathbf{s}_{\text{given}}$   
**end if**  
return:  $\mathbf{s}$ 

---

the step. This means that to be consistent, all the quantities used in the TR must be in the epoch basis, as in Eq. (36). Fundamentally, if we update the TR using the information in the epoch basis (e.g. the length of the step) we should still be able to apply Fletcher’s algorithm.<sup>51</sup> Additionally, because the different epochs bases represent different coordinate transformations, we cannot simply carry over the TR between epochs. Thus, the decision to use the step size from the most recent line search step is therefore an important decision.

#### 2.2.4 Line-Search

At least one iteration of steepest descent (or preconditioned steepest descent) is necessary before beginning quasi-Newton steps since the L-BFGS hessian construction requires information about the previous steps and gradient differences. We have implemented a line search to determine the step size,  $\alpha^{(k)}$ , in this case. The line search is also a fall-back to handle possible problems that can come up, as described later. To reduce the number of Fock builds required for the line search, we use an approximate line search by finding the step size that minimizes a 3rd order polynomial fitted to the energy along the search direction using the energy and gradient at two points in  $\kappa$ -space. One of these points is always the current MOs ( $\kappa = \mathbf{0}$ ), and the other is a scalar multiple of the search direction. Choosing the second fitting point at a reasonable distance from the current point is crucial for the success of the line search. We use a method based on the periodicity of the exponential function.<sup>58</sup> The eigenvalues of the step direction in  $\kappa$ -space, as a matrix (or set of matrices for spin unrestricted), are computed. Then the maximum frequency  $\omega_{\max}$  is determined as the maximum of the absolute values of the eigenvalues. The fitting point along the search direction is then computed as the search direction times a step length, calculated as below.<sup>58</sup>

$$\alpha_{\text{fit}} = \frac{2\pi}{q|\omega_{\max}|} \tag{38}$$

Here  $q$  is the assumed function order, which we choose to be 4. This is a reasonable choice for Hartree-Fock, but for KS-DFT it is more approximate.

The approximate line search method requires only two Fock builds since both the energy and the gradient are easily computed from the Fock matrix. Notice that this means only 1 more Fock build is required than an acceptable quasi-Newton step since the current Fock matrix should already have been computed from the previous iteration. A similar procedure has recently been used,<sup>32</sup> and a nearly identical method for the step determination also has precedent.<sup>41</sup> The energy along the line search direction is a function of the step size,  $E(\alpha)$ , and the 3rd order fit is defined by four parameters:  $a$ ,  $b$ ,  $c$ , and  $d$ .

$$E(\alpha) \approx \hat{E}(\alpha) = a\alpha^3 + b\alpha^2 + c\alpha + d \tag{39}$$

Here  $\hat{E}(\alpha)$  is the fitted polynomial. The coefficients are found by requiring the four conditions to be satisfied (energy and gradient correct at  $\kappa = \mathbf{0}$  and the second point). The minimum is determined by finding the roots of the derivative, which is a simple quadratic polynomial.

$$\hat{E}'(\alpha) = 3a\alpha^2 + 2b\alpha + c \tag{40}$$

Since it is possible to have two solutions to this equation, it is required that  $\alpha > 0$  AND the second derivative of  $\hat{E}(\alpha)$  is positive. If both roots fail to meet these conditions then the fitting is repeated with fitting points that give smaller sample step sizes. We have used a “line search adjustment factor” of 0.5 for this re-fitting. In the case when the 3rd order fit to the energy is so bad that the energy actually increases, the step is rejected and a new fitting range is determined. Assuming that the bad fitting is usually caused by a fitting range that is too large, we shrink the fitting range by a factor of 2 when a step is rejected and the line-search is repeated.

### 2.2.5 Initial Guess

The initial guess orbitals are another critical component for rapid SCF convergence. We use an extended-Hückel initial guess,<sup>59</sup> which is constructed in a minimal basis and then projected onto the full orbital basis. The standard Wolfsberg-Helmholtz formula for the off-diagonal elements of the extended-Hückel Hamiltonian is used:<sup>59</sup>  $H_{ij} = K'S_{ij}(H_{ii} + H_{jj})/2$ , but with the updated formula for the constant  $K'$ .<sup>60</sup> Instead of experimental ionization potentials for the diagonal elements, we follow a suggestion by Lehtola<sup>61</sup> and use numerical Hartree-Fock orbital energies<sup>62</sup> for each shell. Although the guess orbitals are populated according to the Aufbau principle using the extended-Hückel energies and in the minimal basis, after projection to the orbital basis the populations may not be qualitatively correct. When this situation occurs, and the symmetry of the orbitals is such that there is no gradient between incorrectly occupied and incorrectly unoccupied orbitals, QUOTR will not be able to correct the populations. Therefore, we have added an option to apply a small, random unitary matrix to the initial guess which then allows the solver to rotate the incorrectly occupied orbitals and find the lower energy solution. This random matrix is produced by filling  $\kappa$  with random numbers from a uniform real distribution between -1 and 1 scaled to a particular perturbation strength. The random number generator is seeded to allow for reproducible results.

### 2.2.6 Overall Control

There are a couple of parameters that control the overall SCF solver. In general, second order solvers should not be used unless sufficiently close to the true solution. Additionally, the need to have a sufficiently up-to-date preconditioner means that we need to calculate the “pseudocanonical” orbitals relatively close to the solution. Therefore, we only start using L-BFGS once the maximum element of the gradient drops below the L-BFGS start threshold,  $t_b$ . Additionally, the benefit of having the preconditioner updated once more, very near the solution, is motivation for the history reset threshold,  $t_d$ . Here we drop the history



and recalculate the “pseudocannonical” orbitals when the gradient norm per element drops below this value. When  $t_b$  is tight enough it appears that the history reset is not necessary. These two control conditions are shown in Eq. (41)

$$\left\{ \begin{array}{l} \text{anytime} \quad \|\mathbf{g}^{(k)}\|_\infty > t_b \\ \text{firsttime} \quad \|\mathbf{g}^{(k)}\|/n^2 < t_d \end{array} \right. \quad (41)$$

There are a few other cases which trigger the history reset that are essentially sanity-checks: if  $q^{(k)} > 0$ , the step is uphill, or  $\Delta^{(k)}$  is shrunk below the minimum TR tolerance. These may not be necessary, and may never be triggered. In order to reduce unnecessary computation, the solver tries to determine if the history will be reset as early as possible. Thus, the boolean variable  $R_{\text{hist}}$  is set to true when one of these situations is detected. The situations where a history reset will occur are as follows.

- The gradient is too large ( $\|\mathbf{g}^{(k)}\|_\infty > t_b$ )
- The abs max gradient element is below the reset threshold for the first time
- The TR is too small ( $\Delta^{(k)} < t_t$ )
- The step is “up hill” ( $\tilde{\mathbf{s}}^{(k)} \cdot \bar{\mathbf{g}}^{(k)} > 0$ )
- The quadratic model predicts energy increase ( $q^{(k)} > 0$ )

The first 3 of these situations are detected before the L-BFGS step is constructed, allowing the solver to skip this step to go directly to re-building the preconditioner and on to line search. The last 2 situations are only determined after the step is calculated.

All the parameters for QUOTR (other than those inside the TR solver) are listed in Table 2.

Table 2: Parameters for QUOTR

Description	Symbol(s)	Value
extended-Hückel params	-	HF IPs <sup>62</sup>
line-search function order	q	4.0
line-search adjust factor	-	0.5
exponential tolerance	$t_e$	$1 \times 10^{-17}$
max history size	$m$	8
history dot threshold	$t_h$	$1 \times 10^{-5}$
regularizer threshold	$t_r$	0.25
minimum TR tolerance	$t_t$	$1 \times 10^{-10}$
L-BFGS start threshold	$t_b$	0.1
History reset threshold	$t_d$	$1 \times 10^{-6}$ [or 0?]
TR step accept <sup>45</sup>	$\tau_1$	0
TR shrink <sup>45</sup>	$\tau_2$	0.25
TR expand <sup>45</sup>	$\tau_3$	0.75
TR shrink factor <sup>45</sup>	$\eta_1$	0.25
TR shrink by step <sup>45</sup>	$\eta_2$	0.5
TR expand other <sup>45</sup>	$\eta_3$	0.8
TR expand factor <sup>45</sup>	$\eta_4$	2.0

### 3 Technical Details

The QUOTR method was implemented in a developmental version of the Massively Parallel Quantum Chemistry (MPQC) version 4 program package.<sup>63</sup> The orbital bases sets used were 6-31G\*,<sup>64–70</sup> 6-31G\*\*,<sup>66</sup> 6-311++G\*\*,<sup>71–74</sup> and def2-TZVPP.<sup>75</sup> Density fitting was done with the def2-SVP-J basis.<sup>76</sup> The extended-Hückel initial guess was constructed in the Huzinaga MINI basis,<sup>77</sup> then projected onto the orbital basis.

Hartree-Fock calculations were performed in Section 4.1 for the G2 set,<sup>78</sup> the geometries for which were obtained from the Gaussian output files on the NIST website<sup>79</sup> with the exception of four systems that were not available with the correct method (MP2=FULL/6-31G\*). For the four systems that were not available from NIST (acetamide, furan, SiH<sub>2</sub>-triplet and 2-butyne) Gaussian 09<sup>80</sup> was used to obtain the geometry. The G2-1 set consists of 55 systems and is a subset of G2-2, which consists of a total of 148 systems.<sup>78</sup> The RH/DIIS implementation in MPQC uses the default of 5 previous Fock matrices for the extrapolation.

The KS-DFT implementation in MPQC uses GauXC<sup>81</sup> for calculation of the exchange-

correlation potentials and energies. The integration grid used for the 1PLW calculations in Section 4.3 was the “ultrafine” grid, which has 99 radial points and 590 angular points. All other KS-DFT calculations used the “superfine” grid which has 250 radial points and 974 angular points for all atoms except hydrogen, which has 175 radial points. The particular parameterization we use for LDA is Slater Exchange with VWN RPA.<sup>82</sup> For the B3LYP calculations on the Cr systems in Section 4.4, we use VWN3 for the correlation functional<sup>82</sup> to match PySCF. The structure of the neuropeptide, 1PLW,<sup>83</sup> was obtained from the Protein Data Bank (PDB).<sup>84</sup>

Calculation using KDIIS<sup>85</sup> for SCF acceleration on the CrC and Cr<sub>2</sub> systems in Section 4.4 were performed with the Orca program system,<sup>86</sup> version 5.0.4.<sup>87</sup> Additionally, the DIIS implementation from Orca was also used for these systems instead of the MPQC version.

Most calculations were run on Virginia Tech’s Advanced Research Computing (ARC) TinkerCliffs cluster.<sup>88</sup>

## 4 Results and Discussion

### 4.1 G2 Data Set

The number of Fock matrix builds ( $N_F$ ) and solver iterations ( $N_I$ ) are the two key metrics that we examine to understand solver performance. In Table 3 we display statistics for these metrics and also compare with two similar direct minimization solvers: ETDM<sup>32</sup> and GDM.<sup>20</sup> Any systems where convergence was not achieved in 256 iterations are removed from the statistical values and enumerated as “no convergence”. The calculations using QUOTR were Hartree-Fock with spin-restricted orbitals (RHF) if the system is a singlet, and with spin-unrestricted orbitals (UHF) in all other cases. For the comparison using 6-31G\*\* basis, QUOTR kept all history (i.e. maximum history size,  $m$ , was same as number of iterations max).

For the comparison with GDM on G2-1, we used the same basis and our initial guess

Table 3: Convergence Statistics for G2 Set

	G2-2/6-31G*		G2-2/6-31G**			G2-1/6-311++G**		
	DIIS	QUOTR	DIIS	QUOTR <sup>a</sup>	ETDM <sup>b</sup>	DIIS	QUOTR	GDM <sup>c</sup>
$N_F$ : mean	12.0	22.5	11.9	19.8	(17)	11.9	21.7	—
$N_F$ : median	12	17	11	17	(17)	11	18	—
$N_F$ : max	27	191	28	100	72	31	99	—
$N_I$ : mean	12.0	15.3	11.9	14.3	—	11.9	15.8	16.3
$N_I$ : median	12	13	11	13	—	11	13	—
$N_I$ : max	27	98	28	64	—	31	73	42
local minima	2	7	2	8	—	1	1	5
no convergence	1	0	1	0	0	1	0	0

<sup>a</sup> PH<sub>3</sub> rerun with tighteter Fock build precision

<sup>b</sup> Exponential Transformation Direct Minimization<sup>32</sup>

<sup>c</sup> Geometric Direct Minimization<sup>20</sup>

was similar. Our convergence criteria was  $1 \times 10^{-9}$  for both the energy difference ( $E_h$ ) and gradient norm per element, while GDM used  $1 \times 10^{-10}$  for the energy difference and  $1 \times 10^{-7}$  for the RMS gradient. However, due to the tighter gradient criteria for QUOTR, all systems were converged in energy difference to tighter than  $1 \times 10^{-10}E_h$ , making the comparison valid. The average number of iterations is very similar, although QUOTR has a higher max (Si<sub>2</sub>). There was only one other system higher than the max for GDM, and that was NO, which took 60 iterations. It is disappointing that we do not have the information on the number of Fock builds used by GDM, which would be a more accurate comparison of overall computational cost. But, QUOTR performs fairly well with a median of 18 Fock builds to converge. Apart from Si<sub>2</sub> and NO, the highest number of Fock builds for QUOTR is for ClO at 40, which is below the maximum number of iterations for GDM. The only system which did not converge for DIIS in 256 iterations was HCO. The local minimum found by QUOTR (relative to DIIS solution) was CO, while the local minimum found by DIIS (relative to QUOTR) was Si<sub>2</sub>.

Next, comparison to ETDM is more difficult for a few reasons. The data presented in Table 3 is for KS-DFT using the PBE functional, used a different basis (double-zeta polarized default of GPAW) and had frozen core orbitals. We used 6-31G\*\* basis for this comparison

because it is a double-zeta basis with polarization functions on all atoms, so should be more similar to the basis used by ETDM than the other two orbital bases we use. For QUOTR only  $\text{PH}_3$  did not converge, but after tightening the Fock build precision it was able to be converged. The average number of iterations (unclear if it is mean or median) reported for ETDM was 17, which compares well with the median of QUOTR.

We will now take a closer look at the results for G2-2/6-31G\*. A breakdown of the convergence statistics for QUOTR on G2-2/6-31G\* is displayed in Table 4. The designation “Before L-BFGS” indicates the statistics are for the purely line search, early iterations before the first use of a Newton step, while the designation “Line Search” refers to all use of line search (which may be triggered later in the SCF process by e.g. the gradient becoming large again). From the results in Table 4 table we see that on average only 7 Fock builds are needed

Table 4: Statistics Breakdown for G2-2/6-31G\*

		median	max	mean
$N_F$	Cumulative	17	191	22.5
	Before L-BFGS	7	19	7.0
	Line Search	7	139	10.2
$N_I$	Cumulative	13	98	15.3
	Before L-BFGS	3	9	3.0
	Line Search	3	22	3.4

before the gradient is small enough that Quasi-Newton steps begin. This is consistent with the average of 3 line search iterations before stating L-BFGS, because each line search takes 2 Fock builds and we need one initial Fock build. These results are mostly an indication of the quality of the initial guess.

A histogram of the number of Fock builds for this data set is displayed in Figure 1. Based on the histogram, we can see that there are only a few outliers. The systems with more than 40 total Fock builds are displayed in Table 5. From this table we notice that many of these are open-shell systems, indicating that QUOTR has a difficult time with this situation.

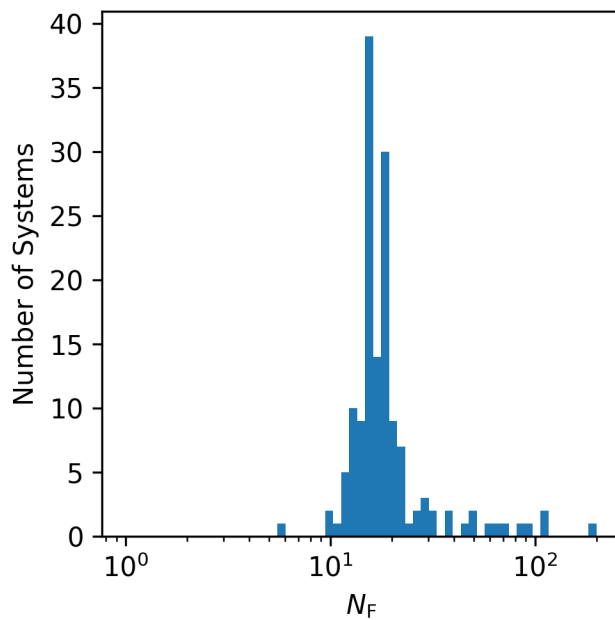


Figure 1:  $N_F$  Histogram using QUOTR for G2-2/6-31G\*

Table 5: Systems with  $N_F > 40$  for G2-2/6-31G\*

System	$N_F$	$N_I$
$\text{BCl}_3$	191	53
$\text{C}_2\text{Cl}_4$	51	37
$\text{CH}_2\text{CHCl}$	68	43
$\text{ClF}_3$	67	57
$\text{H}_2\text{S}$	116	13
$\text{HCl}$	60	12
$\text{HS}$	82	26
$\text{NO}_2$	113	98
$\text{NO}$	92	74
$\text{O}_2$	47	42
$\text{SO}$	50	29

## 4.2 Comparison with Exact Hessian

It is natural to ask how QUOTR compares to using the exact Hessian? We want to know, in terms of  $N_F$ , is it worthwhile to use the exact Hessian, or is L-BFGS sufficient? To make this comparison, we used the Co-iterative augmented Hessian (CIAH)<sup>29</sup> method available in PySCF<sup>89</sup> and counted the number of computational steps equivalent to Fock builds whose statistics are displayed in Table 6. For CIAH the total number of equivalent Fock builds is the sum of the key frames (KF) and coulomb/exchange (JK) calls.<sup>29</sup> The KF enumerate the number of times that the gradient is evaluated exactly, in other cases the gradient is evaluated approximately.<sup>29</sup> It should be noted that the initial guess we use for QUOTR (extended-Hückel) is not the same as that used by CIAH (SOAD from minimal basis), but in Table 6 we consider the comparison fair since each method uses its default guess. Also, the energy is converged much more tightly in QUOTR ( $1 \times 10^{-9} E_h$ ), while CIAH was only converged to  $1 \times 10^{-6} E_h$ .

Table 6:  $N_F$  Statistics for G2-2/6-31G\*

Metric	CIAH	QUOTR	QUOTR <sup>a</sup>
median	30	17	17
mean	35.4	22.5	25.1
max	168	191	191

<sup>a</sup> 14 systems that got local minima re-run with perturbation

For CIAH, one system (HCl) did not converge as it got stuck with a gradient norm of  $1.2 \times 10^{-6}$ , and then simply used 3  $N_F$  per iteration until the max iterations was reached. The system with the next highest  $N_F$  was  $\text{NF}_3$  at 77. The system that took the most Fock builds for QUOTR was  $\text{BCl}_3$  at 191. Looking at the median values in Table 6, we see that QUOTR takes about 1/3 fewer effective Fock builds.

For 14 out of the 148 systems, CIAH got a significantly lower energy than QUOTR (greater than  $1 \times 10^{-9} E_h$ ), and so the comparison with QUOTR might not be considered fair. We reran QUOTR for the 14 systems that were local minima relative to CIAH, but

applied a small, random unitary rotation to the initial guess to break the symmetry. This symmetry breaking allowed all 148 systems to converge to the same (within  $1 \times 10^{-9} E_h$ ) or lower energy as CIAH. The statistics with the corrected 14 systems are displayed in the right most column in Table 6. Notice that the median does not change, and the mean gets a little worse.

To understand how these random perturbations to the initial guess impact convergence, we ran  $\text{AlCl}_3$  (the system with largest error to CIAH) with 50 different seeds for the random number generator. The plot in Figure 2 shows that when the minimum solution is accessible by symmetry, then QUOTR is robust in converging to the solution.

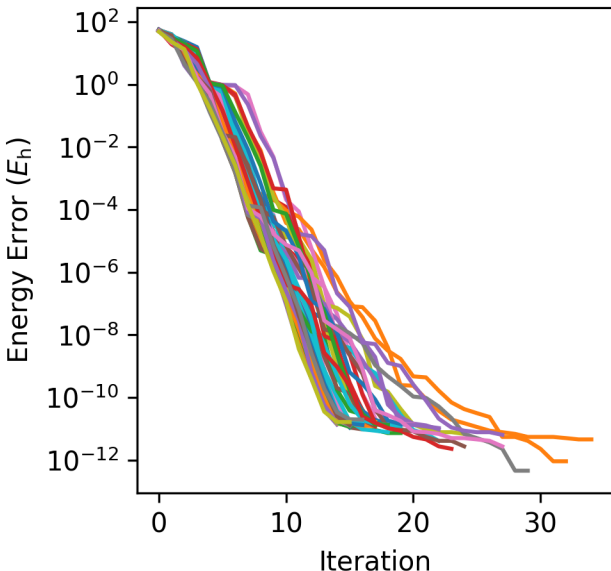


Figure 2: Convergence of  $\text{AlCl}_3$  using QUOTR with random perturbation to guess

To make a comparison starting from exactly the same initial energy, we used the core Hamiltonian guess (“hcore”) because it is unambiguous and we were able to match the initial energy to better than 9 digits between CIAH and QUOTR. The convergence criteria for QUOTR was changed to match the criteria of CIAH, using  $1 \times 10^{-6}$  gradient norm of the unique elements of the gradient. The results for RHF computations of 10 small molecules in the G2 set are displayed in Table 7.



Table 7: Statistics for subset of G2 with hcore guess

System	CIAH			QUOTR
	KF	JK	" $N_F$ "	$N_F$
CH <sub>4</sub>	9	35	44	14
CO	17	70	87	22
F <sub>2</sub>	7	24	31	12
H <sub>2</sub>	3	7	10	5
H <sub>2</sub> O	11	43	54	14
HF	12	48	60	13
Li <sub>2</sub>	6	18	24	10
LiH	5	15	20	10
N <sub>2</sub>	9	34	43	13
NH <sub>3</sub>	12	53	65	19
median	9	34.5	43.5	13
mean	9.1	34.7	43.8	13.2
max	17	70	87	22

From the data in Table 7 we see that in all cases QUOTR is able to converge to the same energy (starting from the same energy) in fewer effective Fock builds. Overall, the median " $N_F$ " required by CIAH is nearly three times as many as required by QUOTR.

### 4.3 Large Calculations

To demonstrate the performance of QUOTR for larger systems, we calculated both HF and LDA solutions for a neuropeptide containing 75 atoms (1PLW).<sup>83</sup> This example shows the robustness of our method as it is one of the systems that a diagonalization based solver could not converge for LDA.<sup>39</sup> In Figure 3 we show convergence of SCF for 1PLW for both HF and LDA using both QUOTR and RH/DIIS. The two panels show two different initial guesses, demonstrating qualitatively similar comparisons between the methods but roughly two times as many iterations for QUOTR in the LDA case. For HF, both methods converge at a similar rate based on iterations. The more difficult case of LDA shows that RH/DIIS oscillates and does not converge, while QUOTR does converge. The reason for the slowness in QUOTR's convergence rate is likely due to the preconditioner shifting. As shown in

Table 8 the LDA calculation is really a zero gap system, and so even near convergence the preconditioner will give a significant shift from the true 1-electron Hessian diagonal. We do apply one later history reset when the gradient norm per element drops below  $1 \times 10^{-6}$  to help make the preconditioner more accurate later in the calculation, and the last recomputation of the preconditioner occurs for “Not Perturbed” calculation at iteration 41 and for the “Perturbed” calculation at iteration 27.

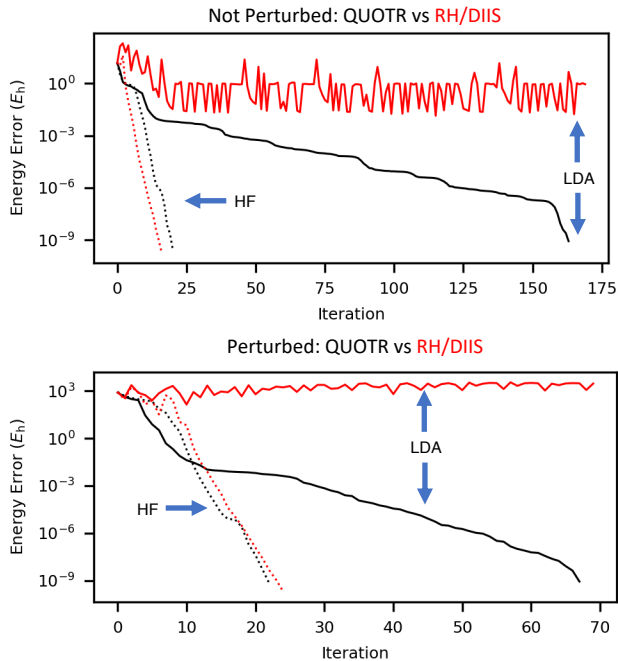


Figure 3: 1PLW Convergence 6-31G\*\*/def2-SVP-J

The converged energies for the HOMO and LUMO along with the gap are displayed in Table 8.

Table 8: Orbital Energies (eV) for 1PLW 6-31G\*\*/def2-SVP-J

	HF	SVWN5	
	Average	unmixed	mixed
HOMO	-6.38	-3.26	-3.26
LUMO	0.86	-3.25	-3.25
Gap	7.24	0.01	0.01

The sizeable gap found for HF is within 0.01 eV of previous work (7.25 eV).<sup>39</sup> For LDA,

the gap turns out to be nearly zero!

## 4.4 Difficult Systems

We have now shown that QUOTR is competitive with standard direct-minimization SCF solvers for simple cases (G2 set), and robust enough to converge nearly zero-gap systems that RH/DIIS cannot converge (1PLW). To investigate both the robustness and efficiency of various SCF solvers we now turn to two small systems that are known to be difficult to converge: Cr<sub>2</sub> and CrC in their singlet states. In Table 9 we display the number of Fock builds necessary to converge SCF using the Orca default convergence criteria of  $5 \times 10^{-5}$  for the gradient norm, and the “hcore” initial guess. Although the “hcore” initial guess is known to be poor, it is one of the only guesses that can easily be consistently constructed by different programs to produce the same initial energy. So, it should be emphasized here that these results are for situations that are doubly difficult: bad initial guess and complicated electronic structure.

Table 9:  $N_F$  hcore guess def2-TZVPP

		QUOTR	TRAH	DIIS <sup>a</sup>	KDIIS <sup>a</sup>	QUOTR <sup>b</sup>	CIAH <sup>b</sup>
CrC	RHF	179	377	44 <sup>c</sup>	47 <sup>c</sup>	222	164 <sup>c</sup>
	B3LYP	129	300	25 <sup>c</sup>	440 <sup>c</sup>	91	240
	LDA	148	202	—	320 <sup>c</sup>	107	208
Cr <sub>2</sub>	RHF	289	295	26 <sup>c</sup>	—	501	160 <sup>c</sup>
	B3LYP	123	267	18 <sup>c</sup>	201 <sup>c</sup>	169	330
	LDA	208	233	20	113 <sup>c</sup>	147	478 <sup>c</sup>

<sup>a</sup> Orca’s implementation

<sup>b</sup> initial guess: hcore + 1 Fock build and diagonalize

<sup>c</sup> local minimum

Comparing QUOTR to TRAH, we see that in all cases QUOTR requires fewer Fock builds. The largest error in converged energies for QUOTR was for CrC with B3LYP, which was higher than TRAH by  $1.1 \times 10^{-6} E_h$ . It should be noted that TRAH uses a random number in one of the Davidson diagonalization start vectors which helps break symmetry,

while for QUOTR we apply a small random unitary rotation to the initial guess to help break symmetry. Thus, the hcore guess is actually not exactly what is used, and the QUOTR initial guess is usually a little higher in energy (  $\sim 1 - 5$  of  $E_h$ ). Additionally, the strength of the random perturbation is important since for the LDA results for  $\text{Cr}_2$  QUOTR converged to a local minimum when the maximum kappa element was 0.001, but increasing it to 0.01 allowed the lower energy solution that matched TRAH to be found.

The results for DIIS and KDIIS look promising from the low number of Fock builds; however, local minima are very common, so these low numbers are deceiving.

For comparison to CIAH, a slightly different version of hcore guess is used, due to PySCF using this different idea of what hcore means. PySCF performs 1 cycle of Fock build then diagonalization for its version of hcore. The initial energy for this guess is generally higher than for the other definition. The first thing to notice is that QUOTR takes more Fock builds than CIAH for RHF, but fewer Fock builds for the other two methods. However, CIAH converges to a local minimum for both systems when using RHF, indicating that QUOTR is providing the more optimal solution.

## 5 Conclusion

We have presented a quasi-Newton direct minimization SCF solver that combines the L-BFGS approximation to the orbital Hessian with the trust-region step restriction method in such a way that the low-rank structure of this Hessian can be efficiently used when solving the trust-region problem. This trust-region quasi-Newton minimization solver (QUOTR) is economical in terms of Fock builds and performs similarly to other solvers. Comparison to an exact Hessian method (CIAH) shows that QUOTR requires far fewer effective Fock builds to reach the same level of convergence. A key advantage of QUOTR (and direct minimization solvers in general) was demonstrated for a biological system where a diagonalization solver was not able to converge. Further work to understand the pathologies of KS-DFT is underway

with QUOTR.

## Acknowledgement

This work was supported by the U.S. Department of Energy via award DE-SC0022327.

## References

- (1) Roothaan, C. C. J. New Developments in Molecular Orbital Theory. *Rev. Mod. Phys.* **1951**, *23*, 69–89.
- (2) McWeeny, R. The Density Matrix in Self-Consistent Field Theory I. Iterative Construction of the Density Matrix. *Proc. R. Soc. Lond. A* **1956**, *235*, 496–509.
- (3) Levy, B.; Berthier, G. Generalized Brillouin Theorem for multiconfigurationalSCF Theories. *Int. J. Quantum Chem.* **1968**, *2*, 307–319.
- (4) Hillier, I. H.; Saunders, V. R. Ab *Initio* Molecular Orbital Calculations of the Ground and Excited States of the Permanganate and Chromate Ions. *Proc. R. Soc. Lond. A* **1970**, *320*, 161–173.
- (5) Hillier, I. H.; Saunders, V. R. A newSCF Procedure and Its Applications Toab Initio Calculations of the States of the Fluorosulphate Radical. *Int. J. Quantum Chem.* **1970**, *4*, 503–518.
- (6) Levy, B. Multiconfiguration Self-Consistent Wavefunctions for CH<sub>4</sub>, C<sub>2</sub>H<sub>4</sub> and C<sub>2</sub>H<sub>6</sub>. *Chemical Physics Letters* **1973**, *18*, 59–62.
- (7) Seeger, R.; Pople, J. A. Self-consistent Molecular Orbital Methods. XVI. Numerically Stable Direct Energy Minimization Procedures for Solution of Hartree–Fock Equations. *J. Chem. Phys.* **1976**, *65*, 265–271.

- (8) Douady, J.; Ellinger, Y.; Subra, R.; Levy, B. Exponential Transformation of Molecular Orbitals: A Quadratically Convergent SCF Procedure. I. General Formulation and Application to Closed-shell Ground States. *J. Chem. Phys.* **1980**, *72*, 1452–1462.
- (9) Pulay, P. Convergence Acceleration of Iterative Sequences. the Case of Scf Iteration. *Chemical Physics Letters* **1980**, *73*, 393–398.
- (10) Bacskay, G. B. A Quadratically Convergent Hartree—Fock (QC-SCF) Method. Application to Closed Shell Systems. *Chem. Phys.* **1981**, *61*, 385–404.
- (11) Bacskay, G. B. A Quadratically Convergent Hartree-Fock (QC-SCF) Method. Application to Open Shell Orbital Optimization and Coupled Perturbed Hartree-Fock Calculations. *Chem. Phys.* **1982**, *65*, 383–396.
- (12) Pulay, P. Improved SCF Convergence Acceleration. *J. Comput. Chem.* **1982**, *3*, 556–560.
- (13) Head-Gordon, M.; Pople, J. A. Optimization of Wave Function and Geometry in the Finite Basis Hartree-Fock Method. *J. Phys. Chem.* **1988**, *92*, 3063–3069.
- (14) Fischer, T. H.; Almlof, J. General Methods for Geometry and Wave Function Optimization. *J. Phys. Chem.* **1992**, *96*, 9768–9774.
- (15) Shepard, R. Elimination of the Diagonalization Bottleneck in Parallel Direct-SCF Methods. *Theoret. Chim. Acta* **1993**, *84*, 343–351.
- (16) Rendell, A. P. Diagonalization-Free SCF. *Chem. Phys. Lett.* **1994**, *229*, 204–210.
- (17) Wong, A. T.; Harrison, R. J. Approaches to Large-Scale Parallel Self-Consistent Field Calculations. *J. Comput. Chem.* **1995**, *16*, 1291–1300.
- (18) Chaban, G.; Schmidt, M. W.; Gordon, M. S. Approximate Second Order Method for Orbital Optimization of SCF and MCSCF Wavefunctions. *Theoretical Chemistry Ac-*

- counts: Theory, Computation, and Modeling (Theoretica Chimica Acta)* **1997**, *97*, 88–95.
- (19) Daniels, A. D.; Scuseria, G. E. Converging Difficult SCF Cases with Conjugate Gradient Density Matrix Search. *Phys. Chem. Chem. Phys.* **2000**, *2*, 2173–2176.
- (20) Van Voorhis, T.; Head-Gordon, M. A Geometric Approach to Direct Minimization. *Molecular Physics* **2002**, *100*, 1713–1721.
- (21) Vandevondele, J.; Hutter, J. An Efficient Orbital Transformation Method for Electronic Structure Calculations. *J. Chem. Phys.* **2003**, *118*, 4365–4369.
- (22) Thøgersen, L.; Olsen, J.; Yeager, D.; Jørgensen, P.; Sałek, P.; Helgaker, T. The Trust-Region Self-Consistent Field Method: Towards a Black-Box Optimization in Hartree–Fock and Kohn–Sham Theories. *J. Chem. Phys.* **2004**, *121*, 16.
- (23) Thøgersen, L.; Olsen, J.; Köhn, A.; Jørgensen, P.; Sałek, P.; Helgaker, T. The Trust-Region Self-Consistent Field Method in Kohn–Sham Density-Functional Theory. *J. Chem. Phys.* **2005**, *123*, 074103.
- (24) Yang, C.; Meza, J. C.; Wang, L.-W. A Trust Region Direct Constrained Minimization Algorithm for the Kohn–Sham Equation. *SIAM J. Sci. Comput.* **2007**, *29*, 1854–1875.
- (25) Sałek, P.; Høst, S.; Thøgersen, L.; Jørgensen, P.; Manninen, P.; Olsen, J.; Jansík, B.; Reine, S.; Pawłowski, F.; Tellgren, E.; Helgaker, T.; Coriani, S. Linear-Scaling Implementation of Molecular Electronic Self-Consistent Field Theory. *J. Chem. Phys.* **2007**, *126*, 114110.
- (26) Weber, V.; Vandevondele, J.; Hutter, J.; Niklasson, A. M. N. Direct Energy Functional Minimization under Orthogonality Constraints. *J. Chem. Phys.* **2008**, *128*, 084113.

- (27) Høst, S.; Olsen, J.; Jansík, B.; Thøgersen, L.; Jørgensen, P.; Helgaker, T. The Augmented Roothaan–Hall Method for Optimizing Hartree–Fock and Kohn–Sham Density Matrices. *J. Chem. Phys.* **2008**, *129*, 124106.
- (28) Baarman, K.; VandeVondele, J. A Comparison of Accelerators for Direct Energy Minimization in Electronic Structure Calculations. *J. Chem. Phys.* **2011**, *134*, 244104.
- (29) Sun, Q. Co-Iterative Augmented Hessian Method for Orbital Optimization. *ArXiv161008423 Phys.* **2017**,
- (30) Helmich-Paris, B. A Trust-Region Augmented Hessian Implementation for Restricted and Unrestricted Hartree–Fock and Kohn–Sham Methods. *J. Chem. Phys.* **2021**, *154*, 164104.
- (31) Nottoli, T.; Gauss, J.; Lipparini, F. A Black-Box, General Purpose Quadratic Self-Consistent Field Code with and without Cholesky Decomposition of the Two-Electron Integrals. *Mol. Phys.* **2021**, *119*, e1974590.
- (32) Ivanov, A. V.; Jónsson, E. Ö.; Vegge, T.; Jónsson, H. Direct Energy Minimization Based on Exponential Transformation in Density Functional Calculations of Finite and Extended Systems. *Comput Phys Commun* **2021**, *267*, 108047.
- (33) Seidl, C.; Barca, G. M. J. Q-Next: A Fast, Parallel, and Diagonalization-Free Alternative to Direct Inversion of the Iterative Subspace. *J. Chem. Theory Comput.* **2022**, *18*, 4164–4176.
- (34) Hall, G. G. The Molecular Orbital Theory of Chemical Valency VIII. A Method of Calculating Ionization Potentials. *Proc. R. Soc. Lond. A* **1951**, *205*, 541–552.
- (35) Anderson, D. G. Iterative Procedures for Nonlinear Integral Equations. *J. ACM* **1965**, *12*, 547–560.



- (36) Harrison, R. J. Krylov Subspace Accelerated Inexact Newton Method for Linear and Nonlinear Equations. *J. Comput. Chem.* **2004**, *25*, 328–334.
- (37) Kollmar, C. The Role of Energy Denominators in Self-consistent Field (SCF) Calculations for Open Shell Systems. *J. Chem. Phys.* **1996**, *105*, 8204–8212.
- (38) Sun, Q. Co-Iterative Augmented Hessian Method for Orbital Optimization. 2017.
- (39) Rudberg, E. Difficulties in Applying Pure Kohn–Sham Density Functional Theory Electronic Structure Methods to Protein Molecules. *J. Phys.: Condens. Matter* **2012**, *24*, 072202.
- (40) Gilbert, A. T. B.; Besley, N. A.; Gill, P. M. W. Self-Consistent Field Calculations of Excited States Using the Maximum Overlap Method (MOM). *J. Phys. Chem. A* **2008**, *112*, 13164–13171.
- (41) Stanton, R. E. The Existence and Cure of Intrinsic Divergence in Closed Shell SCF Calculations. *J. Chem. Phys.* **1981**, *75*, 3426–3432.
- (42) Fletcher, R. Optimization of SCF LCAO Wave Functions. *Mol. Phys.* **1970**, *19*, 55–63.
- (43) Nocedal, J.; Wright, S. J. *Numerical Optimization*, 2nd ed.; Springer Series in Operations Research; Springer: New York, 2006.
- (44) Francisco, J. B.; Martínez, J. M.; Martínez, L. Globally Convergent Trust-Region Methods for Self-Consistent Field Electronic Structure Calculations. *J. Chem. Phys.* **2004**, *121*, 10863.
- (45) Burdakov, O.; Gong, L.; Zikrin, S.; Yuan, Y.-x. On Efficiently Combining Limited-Memory and Trust-Region Techniques. *Math. Prog. Comp.* **2017**, *9*, 101–134.
- (46) Claxton, T. A.; Smith, N. A. Comparison of Minimization Procedures for UHF Wave Functions. *Theoret. Chim. Acta* **1971**, *22*, 399–402.

- (47) Sleeman, D. H. The Determination of SCF LCAO Solutions for Open Shell Configurations. *Theoret. Chim. Acta* **1968**, *11*, 135–144.
- (48) Olsen, J.; Jørgensen, P. Update Methods in Multiconfigurational Self-consistent Field Calculations. *J. Chem. Phys.* **1982**, *77*, 6109–6130.
- (49) Jørgensen, P.; Swannstrom, P.; Yeager, D. L. Guaranteed Convergence in Ground State Multiconfigurational Self-consistent Field Calculations. *J. Chem. Phys.* **1983**, *78*, 347–356.
- (50) Jensen, H.-J. A.; Jørgensen, P. A Direct Approach to Second-order MCSCF Calculations Using a Norm Extended Optimization Scheme. *J. Chem. Phys.* **1984**, *80*, 1204–1214.
- (51) Fletcher, R. *Practical Methods of Optimization*; Wiley: New York, 1980; Vol. Vol. 1.
- (52) Olsen, J.; Yeager, D. L.; Jørgensen, P. In *Advances in Chemical Physics*; Prigogine, I., Rice, S. A., Eds.; John Wiley & Sons, Inc.: Hoboken, NJ, USA, 1983; pp 1–176.
- (53) Thouless, D. Stability Conditions and Nuclear Rotations in the Hartree-Fock Theory. *Nuclear Physics* **1960**, *21*, 225–232.
- (54) Levy, B. Multi-Configuration Self-Consistent Wavefunctions of Formaldehyde. *Chemical Physics Letters* **1969**, *4*, 17–19.
- (55) Helgaker, T.; Jørgensen, P.; Olsen, J. *Molecular Electronic-Structure Theory*, 1st ed.; Helgaker/Molecular Electronic-Structure Theory; John Wiley & Sons, Ltd: Chichester, UK, 2000.
- (56) Moler, C.; Van Loan, C. Nineteen Dubious Ways to Compute the Exponential of a Matrix. *SIAM Rev.* **1978**, *20*, 801–836.

- (57) Byrd, R. H.; Nocedal, J.; Schnabel, R. B. Representations of Quasi-Newton Matrices and Their Use in Limited Memory Methods. *Mathematical Programming* **1994**, *63*, 129–156.
- (58) Abrudan, T.; Eriksson, J.; Koivunen, V. Conjugate Gradient Algorithm for Optimization under Unitary Matrix Constraint. *Signal Processing* **2009**, *89*, 1704–1714.
- (59) Hoffmann, R. An Extended Hückel Theory. I. Hydrocarbons. *J. Chem. Phys.* **1963**, *39*, 1397–1412.
- (60) Ammeter, J. H.; Bürgi, H. B.; Thibeault, J. C.; Hoffmann, R. Counterintuitive Orbital Mixing in Semiempirical and Ab Initio Molecular Orbital Calculations. *J. Am. Chem. Soc.* **1978**, *100*, 3686–3692.
- (61) Lehtola, S. Assessment of Initial Guesses for Self-Consistent Field Calculations. Superposition of Atomic Potentials: Simple yet Efficient. *J. Chem. Theory Comput.* **2019**, *15*, 1593–1604.
- (62) Fischer, C. F. Average-Energy-of-Configuration Hartree-Fock Results for the Atoms Helium to Radon Charlotte Froese Fischer. *Atomic Data and Nuclear Data Tables* **1972**, *4*, 301–399.
- (63) Peng, C.; Lewis, C. A.; Wang, X.; Clement, M. C.; Pierce, K.; Rishi, V.; Pavošević, F.; Slattery, S.; Zhang, J.; Teke, N.; Kumar, A.; Masteran, C.; Asadchev, A.; Calvin, J. A.; Valeev, E. F. Massively Parallel Quantum Chemistry: A High-Performance Research Platform for Electronic Structure. *J. Chem. Phys.* **2020**, *153*, 044120.
- (64) Ditchfield, R.; Hehre, W. J.; Pople, J. A. Self-Consistent Molecular-Orbital Methods. IX. An Extended Gaussian-Type Basis for Molecular-Orbital Studies of Organic Molecules. *J. Chem. Phys.* **1971**, *54*, 724–728.

- (65) Hehre, W. J.; Ditchfield, R.; Pople, J. A. Self—Consistent Molecular Orbital Methods. XII. Further Extensions of Gaussian—Type Basis Sets for Use in Molecular Orbital Studies of Organic Molecules. *J. Chem. Phys.* **1972**, *56*, 2257–2261.
- (66) Hariharan, P. C.; Pople, J. A. The Influence of Polarization Functions on Molecular Orbital Hydrogenation Energies. *Theoret. Chim. Acta* **1973**, *28*, 213–222.
- (67) Dill, J. D.; Pople, J. A. Self-consistent Molecular Orbital Methods. XV. Extended Gaussian-type Basis Sets for Lithium, Beryllium, and Boron. *J. Chem. Phys.* **1975**, *62*, 2921–2923.
- (68) Binkley, J. S.; Pople, J. A. Self-consistent Molecular Orbital Methods. XIX. Split-valence Gaussian-type Basis Sets for Beryllium. *J. Chem. Phys.* **1977**, *66*, 879–880.
- (69) Gordon, M. S.; Binkley, J. S.; Pople, J. A.; Pietro, W. J.; Hehre, W. J. Self-Consistent Molecular-Orbital Methods. 22. Small Split-Valence Basis Sets for Second-Row Elements. *J. Am. Chem. Soc.* **1982**, *104*, 2797–2803.
- (70) Francl, M. M.; Pietro, W. J.; Hehre, W. J.; Binkley, J. S.; Gordon, M. S.; DeFrees, D. J.; Pople, J. A. Self-consistent Molecular Orbital Methods. XXIII. A Polarization-type Basis Set for Second-row Elements. *J. Chem. Phys.* **1982**, *77*, 3654–3665.
- (71) Krishnan, R.; Binkley, J. S.; Seeger, R.; Pople, J. A. Self-consistent Molecular Orbital Methods. XX. A Basis Set for Correlated Wave Functions. *J. Chem. Phys.* **1980**, *72*, 650–654.
- (72) McLean, A. D.; Chandler, G. S. Contracted Gaussian Basis Sets for Molecular Calculations. I. Second Row Atoms,  $Z = 11–18$ . *J. Chem. Phys.* **1980**, *72*, 5639–5648.
- (73) Clark, T.; Chandrasekhar, J.; Spitznagel, G. W.; Schleyer, P. V. R. Efficient Diffuse Function-Augmented Basis Sets for Anion Calculations. III. The 3-21+G Basis Set for First-Row Elements, Li-F. *J. Comput. Chem.* **1983**, *4*, 294–301.

- (74) Spitznagel, G. W.; Clark, T.; von Ragué Schleyer, P.; Hehre, W. J. An Evaluation of the Performance of Diffuse Function-Augmented Basis Sets for Second Row Elements, Na-Cl: Diffuse Function-Augmented Basis Sets. *J. Comput. Chem.* **1987**, *8*, 1109–1116.
- (75) Weigend, F.; Ahlrichs, R. Balanced Basis Sets of Split Valence, Triple Zeta Valence and Quadruple Zeta Valence Quality for H to Rn: Design and Assessment of Accuracy. *Phys. Chem. Chem. Phys.* **2005**, *7*, 3297.
- (76) Weigend, F. Accurate Coulomb-fitting Basis Sets for H to Rn. *Phys. Chem. Chem. Phys.* **2006**, *8*, 1057.
- (77) Schuchardt, K. L.; Didier, B. T.; Elsethagen, T.; Sun, L.; Gurumoorthi, V.; Chase, J.; Li, J.; Windus, T. L. Basis Set Exchange: A Community Database for Computational Sciences. *J. Chem. Inf. Model.* **2007**, *47*, 1045–1052.
- (78) Curtiss, L. A.; Raghavachari, K.; Redfern, P. C.; Pople, J. A. Assessment of Gaussian-2 and Density Functional Theories for the Computation of Enthalpies of Formation. *J. Chem. Phys.* **1997**, *106*, 1063–1079.
- (79) Johnson, RD. Computational Chemistry Comparison and Benchmark Database, NIST Standard Reference Database 101. 2002.
- (80) Frisch, M. J.; Trucks, G. W.; Schlegel, H. B.; Scuseria, G. E.; Robb, M. A.; Cheeseman, J. R.; Scalmani, G.; Barone, V.; Mennucci, B.; Petersson, G. A.; Nakatsuji, H.; Caricato, M.; Li, X.; Hratchian, H. P.; Izmaylov, A. F.; Bloino, J.; Zheng, G.; Sonnenberg, J. L.; Hada, M.; Ehara, M.; Toyota, K.; Fukuda, R.; Hasegawa, J.; Ishida, M.; Nakajima, T.; Honda, Y.; Kitao, O.; Nakai, H.; Vreven, T.; Montgomery, J. A. Jr.; Peralta, J. E.; Ogliaro, F.; Bearpark, M.; Heyd, J. J.; Brothers, E.; Kudin, K. N.; Staroverov, V. N.; Keith, T.; Kobayashi, R.; Normand, J.; Raghavachari, K.; Rendell, A.; Burant, J. C.; Iyengar, S. S.; Tomasi, J.; Cossi, M.; Rega, N.; Millam, J. M.;

- Klene, M.; Knox, J. E.; Cross, J. B.; Bakken, V.; Adamo, C.; Jaramillo, J.; Pomper, R.; Stratmann, R. E.; Yazyev, O.; Austin, A. J.; Cammi, R.; Pomelli, C.; Ochterski, J. W.; Martin, R. L.; Morokuma, K.; Zakrzewski, V. G.; Voth, G. A.; Salvador, P.; Dannenberg, J. J.; Dapprich, S.; Daniels, A. D.; Farkas, O.; Foresman, J. B.; Ortiz, J. V.; Cioslowski, J.; Fox, D. J. Gaussian 09. Gaussian, Inc., 2013.
- (81) Petrone, A.; Williams-Young, D. B.; Sun, S.; Stetina, T. F.; Li, X. An Efficient Implementation of Two-Component Relativistic Density Functional Theory with Torque-Free Auxiliary Variables. *Eur. Phys. J. B* **2018**, *91*, 169.
- (82) Vosko, S. H.; Wilk, L.; Nusair, M. Accurate Spin-Dependent Electron Liquid Correlation Energies for Local Spin Density Calculations: A Critical Analysis. *Can. J. Phys.* **1980**, *58*, 1200–1211.
- (83) Marcotte, I.; Separovic, F.; Auger, M.; Gagné, S. M. A Multidimensional <sup>1</sup>H NMR Investigation of the Conformation of Methionine-Enkephalin in Fast-Tumbling Bicelles. *Biophys. J.* **2004**, *86*, 1587–1600.
- (84) Berman, H. M. The Protein Data Bank. *Nucleic Acids Res.* **2000**, *28*, 235–242.
- (85) Kollmar, C. Convergence Optimization of Restricted Open-Shell Self-Consistent Field Calculations. *Int. J. Quant. Chem.* **1997**, *62*, 617–637.
- (86) Neese, F. The ORCA Program System. *WIREs Comput Mol Sci* **2012**, *2*, 73–78.
- (87) Neese, F. Software Update: The ORCA Program System—Version 5.0. *WIREs Comput Mol Sci* **2022**, *12*.
- (88) TinkerCliffs. <https://www.docs.arc.vt.edu/resources/compute/00tinkercliffs.html>.
- (89) Sun, Q.; Zhang, X.; Banerjee, S.; Bao, P.; Barbry, M.; Blunt, N. S.; Bogdanov, N. A.; Booth, G. H.; Chen, J.; Cui, Z.-H.; Eriksen, J. J.; Gao, Y.; Guo, S.; Hermann, J.;

Hermes, M. R.; Koh, K.; Koval, P.; Lehtola, S.; Li, Z.; Liu, J.; Mardirossian, N.; McClain, J. D.; Motta, M.; Mussard, B.; Pham, H. Q.; Pulkin, A.; Purwanto, W.; Robinson, P. J.; Ronca, E.; Sayfutyarova, E. R.; Scheurer, M.; Schurkus, H. F.; Smith, J. E. T.; Sun, C.; Sun, S.-N.; Upadhyay, S.; Wagner, L. K.; Wang, X.; White, A.; Whitfield, J. D.; Williamson, M. J.; Wouters, S.; Yang, J.; Yu, J. M.; Zhu, T.; Berkelbach, T. C.; Sharma, S.; Sokolov, A. Y.; Chan, G. K.-L. Recent Developments in the P  $\gamma$  SCF Program Package. *J. Chem. Phys.* **2020**, *153*, 024109.

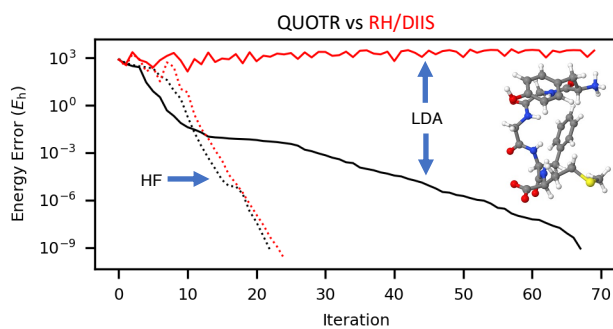


Figure 4: For Table of Contents Only